Geochemistry Geophysics Geosystems G3

Article
Volume 14, Number 8
22 August 2013
doi: 10.1002/ggge.20188
ISSN: 1525-2027

Published by AGU and the Geochemical Society

Major and trace element composition of the high $^{3}He/^{4}He$ mantle: Implications for the composition of a nonchonditic Earth

Matthew G. Jackson
Department of Earth Science, University of California, Santa Barbara, California, 93109-9630, USA (jackson@geol.ucsb.edu)

A. Mark Jellinek
Department of Earth, Ocean and Atmospheric Sciences, University of British Columbia, Vancouver, British Columbia, Canada

[1] The bulk composition of the silicate portion of the Earth (BSE) has long been assumed to be tied to chondrites, in which refractory, lithophile elements like Sm and Nd exist in chondritic relative abundances. However, the $^{142}Nd/^{144}Nd$ ratios of modern terrestrial samples are 18 ± 5 ppm higher than the ordinary-chondrite reservoir, and this challenges the traditional BSE model. Here we investigate a hypothesis that this terrestrial ^{142}Nd excess is related to a Sm/Nd ratio 6% higher than chondritic. This Sm/Nd ratio yields a superchondritic $^{143}Nd/^{144}Nd$ ($\sim$0.5130) similar to that identified in the highest $^{3}He/^{4}He$ mantle reservoir, and we argue that this reservoir represents the BSE composition for lithophile elements. We develop a compositional model for BSE in which the elevated Sm/Nd requires a shift of $^{143}Nd/^{144}Nd$ from 0.51263 (chondritic) to 0.51300. The new BSE composition is depleted in highly incompatible elements, including K, relative to the chondrite-based BSE, and offers a solution the "missing" ^{40}Ar paradox. This BSE compositional model requires that >83% of the mantle is depleted to form continental crust. It also implies a $\sim$30% reduction in BSE U, Th and K, and therefore in the current rate of radiogenic heating and, thus, a proportional increase in the heat flow delivered to surface by plate tectonics. We explore thermal history models including effects related to a newly recognized evolution in the style of plate tectonics over Earth history: The lower radiogenic heat production may delay the onset of core convection and dynamo action to as late as 3.5 Gyr.

Components: 17,857 words, 7 figures, 4 tables.

Keywords: primitive mantle; bulk silicate Earth; mantle geochemistry; missing Ar; ^{142}Nd; chondrite; SCHEM; nonchondritic Earth; $^{3}He/^{4}He$.

Index Terms: 1000 Geochemistry; 1009 Geochemical modeling; 1040 Radiogenic isotope geochemistry; 1038 Mantle processes; 1025 Composition of the mantle; 1065 Major and trace element geochemistry; 3600 Mineralogy and Petrology; 3610 Geochemical modeling; 3621 Mantle processes; 8400 Volcanology; 8410 Geochemical modeling.

Received 26 February 2013; **Revised** 23 May 2013; **Accepted** 28 May 2013; **Published** 22 August 2013.

Jackson, M. G., and A. M. Jellinek (2013), Major and trace element composition of the high $^{3}He/^{4}He$ mantle: Implications for the composition of a nonchonditic Earth, *Geochem. Geophys. Geosyst., 14*, 2954–2976, doi:10.1002/ggge.20188.

1. Introduction

[2] The Earth's mantle preserves a history of the long-term evolution and differentiation of the planet. For example, mid-ocean ridge basalts (MORB) exhibit geochemical signatures of incompatible element depletion, and indicate that much of the upper mantle has experienced melt removal over geologic time [*Gast*, 1968; *Hofmann*, 1988; *Salters and Stracke*, 2004; *Workman and Hart*, 2005; *Boyet and Carlson*, 2006]. The mantle is "re-enriched" when crust, both oceanic and continental, are subducted into the mantle, and the geochemistry of basalts erupted at some oceanic hotspots record the return of these subducted components, as well as deeply seated primitive components, in regions of mantle upwelling and melting [*Zindler and Hart*, 1986; *Hofmann*, 1997; *White*, 2010]. These enriched and depleted mantle reservoirs are mixed, thereby complicating much of the geochemical history recorded in the mantle [e.g., *Brandenburg et al*., 2008; *van Keken et al*., 2004]. While much of the mantle has been processed at mid-ocean ridges and subduction zones, fundamental questions remain: Are there domains in the mantle that have survived, relatively undisturbed since accretion, that might shed light on the composition of the earliest Earth? If so, what are their compositions?

[3] Helium is an important tracer for primitive material residing in the Earth's mantle. Helium has two stable isotopes: ^{3}He, which is of primordial origin in the mantle, and ^{4}He, which has both radiogenic (resulting primarily from U and Th decay) and primordial components in the Earth's mantle. Lavas with high ^{3}He/^{4}He have long been thought to represent melts of relatively undegassed regions of the mantle with low (Th+U)/He ratios, which are conducive to preserving high ^{3}He/^{4}He over geologic time [e.g., *Kurz et al*., 1982, 1983; *Farley et al*., 1992; *Stuart et al*., 2003; *Class and Goldstein*, 2005]. Lavas with the highest terrestrial mantle ^{3}He/^{4}He globally, from Baffin Island [*Stuart et al*., 2003] and West Greenland [*Graham et al*., 1998], exhibit Pb-isotopic compositions that lie near the geochron, the locus of data in Pb-isotopic space that have had undisturbed U/Pb ratios for ~4.5 Ga [*Jackson et al*., 2010; *Jackson and Carlson*, 2011]. This observation is consistent with the high ^{3}He/^{4}He mantle being the oldest accessible terrestrial mantle reservoir. This interpretation is supported by the discovery that the high ^{3}He/^{4}He mantle sampled by the Iceland hotspot (which sourced Baffin Island lavas at ~62 Ma) [*Storey et al*., 1998] has ^{129}Xe/^{130}Xe isotopic compositions distinct from the depleted MORB mantle (DMM), which requires formation and separation of the DMM and high ^{3}He/^{4}He reservoirs within ~100 Ma following accretion [*Mukhopadhyay*, 2012]. In contrast to the primitive He and Pb isotopic compositions in the highest ^{3}He/^{4}He lavas, their ^{143}Nd/^{144}Nd isotopic compositions are higher than chondritic [e.g., *Hart et al*., 1992; Hanan and Graham, 1996], with values closer to the average ^{143}Nd/^{144}Nd of the MORB mantle (0.51313) [Su, 2003] than chondritic (0.51263) [*Bouvier et al*., 2008]. If the bulk silicate Earth (BSE) originated by accretion of chondrites, or planetesimals that descended from chondritic precursors, then the superchondritic ^{143}Nd/^{144}Nd and ^{176}Hf/^{177}Hf ratios in high ^{3}He/^{4}He lavas [e.g., *Caro and Bourdon*, 2010; *Jackson et al*., 2010] suggest a history of depletion by melt extraction, a process that increases the Lu/Hf and Sm/Nd ratios in the melt-depleted residue. The association of primitive noble gas isotopic signatures in a mantle reservoir with distinctly nonchondritic refractory element radiogenic isotopic signatures is a paradox that has been the subject of considerable discussion [e.g., *Kurz et al*., 1982; *Hart et al*., 1992; *Class and Goldstein*, 2005; *Parman et al*., 2005; *Caro et al*., 2008; *Carlson and Boyet*, 2008; *Gonnermann and Mukhopadhyay*, 2009; *Caro and Bourdon*, 2010; *Jackson et al*., 2010; *Jackson and Carlson*, 2011].

[4] A recent landmark discovery provides a possible solution to this helium paradox. *Boyet and Carlson* [2005] (BC05 hereafter) found small, but significant differences (18 ± 5 ppm) [*Carlson and Boyet*, 2008] in ^{142}Nd/^{144}Nd between modern terrestrial samples and ordinary (O) and carbonaceous (C)-chondrites. This difference is important because, if the Earth has chondritic ratios of Sm/Nd, then the Earth is predicted to have ^{142}Nd/^{144}Nd and ^{143}Nd/^{144}Nd identical to chondrites. BC05 suggest that the ^{142}Nd excess in terrestrial samples relative to O and C-chondrites is the result of ^{146}Sm decay, and that the accessible silicate Earth has superchondritic Sm/Nd and ^{143}Nd/^{144}Nd (0.5130 ± 0.0001). This value matches the ^{143}Nd/^{144}Nd ratios measured in high ^{3}He/^{4}He lavas, and has lead to the idea that the high ^{3}He/^{4}He reservoir may reflect the lithophile element composition of a nonchondritic BSE [*Caro et al*., 2008; *Jackson et al*., 2010] from which most of the continental crust and all known oceanic lavas were derived [*Jackson and Carlson*, 2012]. In this paper, chondrite-based models for BSE are those models in which only the refractory

lithophile elements (like Sm and Nd) exist in chondritic relative abundances, while ratios of other elements (e.g., volatile element/refractory element, siderophile element/lithophile element, etc.) may not. The term "nonchondritic Earth," as used here, implies that even the refractory lithophile elements fail to exhibit chondritic relative abundances.

[5] An alternative model for the ^{142}Nd excess in terrestrial samples relative to O and C-chondrites suggests that it is the result of Earth's accreting from a nucleosynthetically heterogeneous early solar nebula [*Ranen and Jacobsen*, 2006; *Kleine et al*., 2013], a view challenged by recent high-precision measurements of Ba, Sm, Nd, and Sr isotopes in chondrites [*Andreasen and Sharma*, 2006, 2007; *Carlson et al*., 2007; *Carlson and Boyet*, 2008; *Qin et al*., 2011]. While some enstatite (E)-chondrites have been found to exhibit ^{142}Nd/^{144}Nd similar to the Earth [*Gannoun et al*., 2011], their ^{143}Nd/^{144}Nd is similar to O and C-chondrites and does not provide a solution to the paradox of superchondritic ^{143}Nd/^{144}Nd in terrestrial lavas with primitive ^{3}He/^{4}He, and we do not explore an E-chondrite model for the Earth [e.g., *Javoy et al*., 2010]. However, we note that the community cannot, at present, rule out an E-chondrite model for the BSE or demonstrate the Earth accreted from E-chondrites, and this will no doubt continue to be a source of discussion.

[6] Here we explore the implications for ^{146}Sm decay driving the ^{142}Nd/^{144}Nd difference between Earth and O and C-chondrites. If the difference is the result of ^{146}Sm decay, then the accessible Earth (i.e., crustal and upper mantle rocks and MORB and hotspot lavas) [e.g., *Jackson and Carlson*, 2012] did not have chondritic relative abundances of the refractory lithophile elements, including Sm/Nd, during the first ~20 million years (using the ^{146}Sm half-life [68 Ma] from *Kinoshita et al*. [2012]) after accretion (BC05). Instead, the observation of constant superchondritic ^{142}Nd/^{144}Nd in all modern terrestrial mantle reservoirs requires that they descend from a parental reservoir that has a Sm/Nd ratio ~4.5–7.9% higher than chondrites [e.g., *Jackson and Carlson*, 2012], but the origin of this reservoir is debated. In an attempt to preserve the chondrite model for BSE in light of the new ^{142}Nd result, BC05 suggest that an early (ca., <30 Ma following accretion, where they assumed a 103 Ma half-life for ^{146}Sm) differentiation event of a chondritic Earth resulted in two reservoirs: an early depleted reservoir (EDR) with Sm/Nd 4.5–7.9% higher than chondrites from which all modern terrestrial mantle reservoirs descend, and a complementary early enriched reservoir (EER) hidden in the deep mantle with characteristics similar to that proposed by *Labrosse et al*. [2007]. To-date, however, all measured modern MORB and hotspot lavas have the same ^{142}Nd/^{144}Nd as the terrestrial standard [e.g., *Boyet and Carlson*, 2006; *Caro et al*., 2006; *Andreasen et al*., 2008; *Murphy et al*., 2010; *Jackson and Carlson*, 2012]. There is no observational evidence from geochemistry for an EER, but its existence cannot be excluded. However, to avoid the requirement of a hidden EER at the bottom of the mantle, *O'Neill and Palme* [2008] suggest that the mantle began with a chondritic composition that underwent early catastrophic differentiation and loss of early-formed enriched crust by impact erosion. Alternatively, impact erosion-induced loss of enriched crust from the planetesimals that accreted to make up the Earth could generate a BSE composition with superchondritic Sm/Nd. In the impact erosion model, the residual BSE (or the impact-eroded planetesimals that accreted to form the Earth), depleted in the highly incompatible elements by early loss of enriched crust to space, hosts a bulk superchondritic Sm/Nd ratio and is compositionally identical to BC05's EDR (but the BC05 EER has been lost to space instead of the deep mantle).

[7] This early-formed, depleted reservoir with superchondritic ^{142}Nd/^{144}Nd and ^{143}Nd/^{144}Nd has been argued to be the most primitive surviving reservoir in the Earth's mantle and host to high ^{3}He/^{4}He [*Carlson and Boyet*, 2008; *Caro et al*., 2008; *Caro and Bourdon*, 2010; *Jackson et al*., 2010; *Jackson and Carlson*, 2011]. Lavas with the highest terrestrial mantle ^{3}He/^{4}He have superchondritic ^{143}Nd/^{144}Nd ratios that generally fall within the range of values predicted for the EDR (i.e., 0.5130 ± 0.0001). Importantly, like all modern terrestrial mantle-derived lavas measured to-date, lavas with high ^{3}He/^{4}He have ^{142}Nd/^{144}Nd that is 18 ± 5 ppm higher than O and C-chondrites [*Andreasen et al*., 2008; *Murphy et al*., 2010; *Jackson and Carlson*, 2012]. Therefore, we adopt the recent hypothesis that the mantle reservoir with high ^{3}He/^{4}He was formed by early melt extraction from O or C-chondrite precursors and is the parental reservoir from which all accessible modern terrestrial mantle reservoirs were derived [*Carlson and Boyet*, 2008; *Caro et al*., 2008; *Caro and Bourdon*, 2010; *Jackson et al*., 2010; *Jackson and Carlson*, 2012].

[8] Taking the high ^{3}He/^{4}He mantle to be the most primitive accessible terrestrial mantle reservoir, we develop a major and trace element

compositional model for this reservoir that is consistent with Nd-isotopic constraints, which require early formation of the high $^{3}He/^{4}He$ mantle and a Sm/Nd ratio that is 4.5–7.9% higher than chondritic. Therefore, our model for the high $^{3}He/^{4}He$ mantle provides a lithophile element composition for either a nonchondritic BSE (if BSE is not chondritic owing to early loss of enriched material to space), or the EDR (if BSE is chondritic and enriched material is hidden in the deep mantle). This manuscript is meant to complement the work of *Caro and Bourdon* [2010], and the new compositional model for the high $^{3}He/^{4}He$ mantle provides a major and trace element composition for a nonchondritic BSE that is based on the composition of high $^{3}He/^{4}He$ lavas, called Super-Chondritic Earth Model (SCHEM).

[9] To construct the high-$^{3}He/^{4}He$ mantle compositional model for the lithophile element abundances in nonchondritic BSE, we first use *Caro and Bourdon's* [2010] work to show that superchondritic $^{143}Nd/^{144}Nd$ in BSE also requires different $^{176}Hf/^{177}Hf$ and $^{87}Sr/^{86}Sr$ ratios (section 2.1). This choice requires revision of the BSE parent-daughter ratios for these isotopic systems (section 2.1), which, in turn, enables us to construct the "backbone" of the normalized trace element pattern, also known as a spidergram, of the high $^{3}He/^{4}He$ mantle (section 2.2). Using further isotopic constraints and canonical trace element ratios, we complete the spidergram with additional trace elements (sections 2.3–2.4), and we anchor the spidergram to the estimated concentration of Lu (~0.064 ppm; section 2.5) as this element exhibits little variability between different chondrite-based compositional models for the BSE (e.g., 0.068–0.0711 ppm) [e.g., *McDonough and Sun*, 1995, MS95 hereafter; *Palme and O'Neil*, 2003; *Hart and Zindler*, 1986] and estimates for DMM (0.058–0.063 ppm) [*Salters and Stracke*, 2004; *Workman and Hart*, 2005; *Boyet and Carlson*, 2006]. We bracket the range of major element compositions of the high $^{3}He/^{4}He$ mantle (section 2.6). We discuss uncertainties associated with the compositional estimate for this mantle reservoir (section 3) and we show that, using simple melting models, this mantle composition can generate a melt with a trace element pattern similar to that measured in the highest $^{3}He/^{4}He$ lavas (section 4). Finally, we show that the trace element budget satisfies geochemical constraints for the formation of continental crust, provides a possible solution to the long-standing "missing Ar" paradox, and is consistent with plausible models for the thermal evolution of the Earth, which predict a delayed onset of core convection and dynamo action (section 5).

2. Estimating the Lithophile Element Composition of a Nonchondritic BSE by Constructing the Trace Element Budget of the High $^{3}He/^{4}He$ Mantle

2.1. Calculating the ^{147}Sm-^{143}Nd, ^{176}Lu-^{176}Hf, and ^{87}Rb-^{87}Sr of the high $^{3}He/^{4}He$ mantle

[10] At the foundation of our trace element model is the assumption that a nonchondritic BSE has a Sm/Nd ratio 4.5–7.9% higher than chondritic, which is necessary to generate the 18 ± 5 ppm difference in $^{142}Nd/^{144}Nd$ between chondrites and modern terrestrial mantle-derived lavas by ^{146}Sm decay. The uncertainty in $^{142}Nd/^{144}Nd$, from 13 to 23 ppm higher than chondritic, results in uncertainty in the Sm/Nd ratio, which propagates into uncertainty in the $^{143}Nd/^{144}Nd$ ratio. Therefore, assuming an initial $^{143}Nd/^{144}Nd$ that is chondritic and closed-system evolution for 4.567 Ga, the range of possible Sm/Nd ratios will generate a range of present-day $^{143}Nd/^{144}Nd$ values of 0.5130 ± 0.0001 ($\varepsilon^{143}Nd = 7.1 \pm 2.0$). This range of $^{143}Nd/^{144}Nd$ values for a nonchondritic BSE is similar to the range of values identified in the highest $^{3}He/^{4}He$ lavas globally [*Stuart et al.*, 2003; *Jackson et al.*, 2007; *Starkey et al.*, 2009], and we argue that the lithophile element composition of the high $^{3}He/^{4}He$ mantle represents the composition of a nonchondritic BSE.

[11] *Caro and Bourdon* [2010] use the superchondritic $^{147}Sm/^{144}Nd$ and $^{143}Nd/^{144}Nd$ of the high $^{3}He/^{4}He$ mantle to estimate its $^{176}Lu/^{176}Hf$ and $^{87}Rb/^{87}Sr$ ratios. The lithophile, incompatible behavior of Sm-Nd, Lu-Hf, and Rb-Sr systems during melting and subsequent magmatic differentiation cause the isotopic systematics of $^{143}Nd/^{144}Nd$, $^{176}Hf/^{177}Hf$, and $^{87}Sr/^{86}Sr$ to exhibit correlated variations in crustal and mantle-derived samples [e.g., *Allègre et al.*, 1979; *DePaolo and Wasserburg*, 1979; *DePaolo*, 1980; *Patchett et al.*, 1981; *Salters and Hart*, 1991; *Vervoort et al.*, 1999; *Chauvel et al.*, 2008; *Bouvier et al.*, 2008; *Caro and Bourdon*, 2010]. Consequently, a key assumption for evaluating the Sr and Hf isotopic composition of BSE is that the correlated global isotopic data—which form "mantle arrays" in $^{143}Nd/^{144}Nd$ versus $^{176}Hf/^{177}Hf$ and $^{143}Nd/^{144}Nd$

vs. $^{87}Sr/^{86}Sr$ isotopic spaces—pass through BSE (Figure 1). Therefore, if the composition of a nonchondritic BSE is known for any one of these three isotopic systems (e.g., $^{143}Nd/^{144}Nd$), then its composition can be estimated for the other two isotopic systems ($^{87}Sr/^{86}Sr$ and $^{176}Hf/^{177}Hf$) using the mantle array. In a plot of $\varepsilon^{143}Nd$ versus $\varepsilon^{176}Hf$, the range of Nd-isotopic compositions for nonchondritic BSE ($\varepsilon^{143}Nd = 7.1 \pm 2.0$) intersects the mantle array over a range of $\varepsilon^{176}Hf$ values ($\varepsilon^{176}Hf = 12.6 \pm 3.1$), and these are the Hf-isotope values used for modeling the trace element composition of a nonchondritic BSE (Figure 1 and Table 1). In $^{87}Sr/^{86}Sr$ versus $^{143}Nd/^{144}Nd$ isotopic space, the range of $^{143}Nd/^{144}Nd$ values for a nonchondritic BSE intersects the mantle array over a range of $^{87}Sr/^{86}Sr$ values (0.7030 ± 0.0004) (Table 1). The $^{143}Nd/^{144}Nd$, $^{176}Hf/^{177}Hf$, and $^{87}Sr/^{86}Sr$ isotopic values selected for a nonchondritic BSE in Table 1 are similar to those presented for SCHEM by *Caro and Bourdon* [2010].

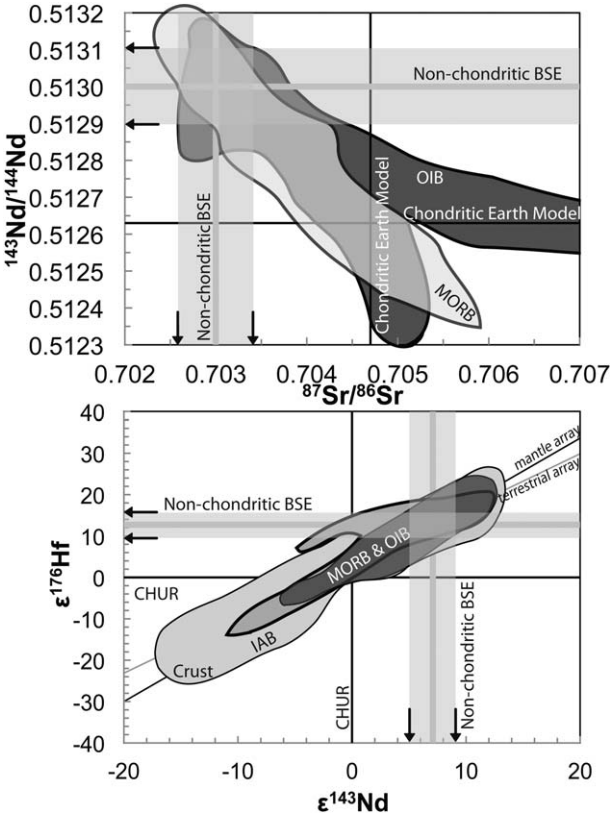

Figure 1. The radiogenic isotopic compositions for lavas from OIB and MORB show clear arrays in (top) $^{87}Sr/^{86}Sr$ versus $^{143}Nd/^{144}Nd$ and (bottom) $\varepsilon^{143}Nd$ versus $\varepsilon^{176}Hf$ isotopic spaces. The trends in the data, called "mantle arrays," are assumed to pass through BSE. If BSE has chondritic $^{143}Nd/^{144}Nd$ (0.51263) [*Bouvier et al*., 2008], then the $^{87}Sr/^{86}Sr$ and $^{176}Hf/^{177}Hf$ of the BSE can be calculated by extrapolation from the mantle array. Similarly, if the BSE is nonchondritic, and has a composition like the nonchondritic BSE in Table 1, then the $^{143}Nd/^{144}Nd$ of the nonchondritic BSE (0.5130 ± 0.0001) can be used to estimate its $^{87}Sr/^{86}Sr$ (lower than the chondrite-based BSE estimate) and $^{176}Hf/^{177}Hf$ (higher). The figures are modified from *Caro and Bourdon* [2010]. See section 2.1 and Table 1 for details.

2.2. Constructing the "Backbone" of the High $^{3}He/^{4}He$ Mantle Spidergram: Toward a Composition of a Nonchondritic BSE

[12] Armed with estimates for the Nd, Hf and Sr isotopic compositions of a nonchondritic BSE, it is possible to calculate the present-day parent-daughter ratios of these three isotopic systems assuming closed-system isotopic evolution for 4.567 Ga, an age that is consistent with Pb [*Jackson et al*., 2010] and Xe [*Mukhopadhyay*, 2012] isotopic measurements on high $^{3}He/^{4}He$ lavas from Baffin Island and the associated Iceland hotspot. We follow *Caro and Bourdon* [2010] and *Jackson et al*. [2010] and assume that the initial Nd, Hf, and Sr isotopic compositions and associated parent-daughter ratios of BSE (or the planetesimals that differentiated before accreting to form the Earth) were chondritic. The parent-daughter ratios required to generate the present-day isotopic compositions of the nonchondritic BSE result in Sm/Nd (0.3441 instead of the chondritic value of 0.324), Lu/Hf (0.266 instead of 0.237) and Rb/Sr (0.0211 instead of 0.029) ratios that are different from that predicted by the chondrite-based model for BSE (Table 1).

[13] The three isotopically constrained parent-daughter ratios bracket the entire spidergram: The Rb/Sr ratio brackets the portion of the spidergram occupied by trace elements that are most incompatible during mantle melting, the Sm/Nd ratio brackets the moderately incompatible elements, and the Lu/Hf ratio brackets the least incompatible elements. These three segments of the spidergram can be "linked" together using canonical ratios derived from measurement of oceanic lavas (Figure 2). Incompatible trace elements that have the same partition coefficients during mantle melting exhibit reasonably constant ratios in oceanic lavas independent of the absolute concentrations in the lavas (as long as the degree of melting is much larger than the bulk partition coefficient), and these canonical ratios are considered to reflect the mantle source of the lavas [*Hofmann*, 2003]. A number of ratios are employed in this study to construct the spidergram of the nonchondritic BSE

Table 1. ^{147}Sm-^{143}Nd, $^{176}Lu/^{176}Hf$, $^{87}Rb/^{86}Sr$ for the Nonchondritic BSE, Which Represents the High $^{3}He/^{4}He$ Mantle Composition[a]

					Nonchondritic BSE	Nonchondritic BSE	Nonchondritic BSE
	Chondrite-Based BSE (CHUR)	DMM [WH05]	DMM [SS04]	DMM [BC06]	High $^{3}He/^{4}He$ Mantle (This Study)	High $^{3}He/^{4}He$ Mantle enriched (This Study)	High $^{3}He/^{4}He$ Mantle depleted (This Study)
$^{143}Nd/^{144}Nd$	0.512630	0.51313	0.51311	0.51313	0.51300	0.51290	0.51310
$^{147}Sm/^{144}Nd$	0.1960	0.249	0.229	0.216	0.2081	0.2047	0.2114
Sm/Nd	0.324	0.411	0.379	0.358	0.3441	0.3386	0.3497
$\varepsilon^{143}Nd$ (versus CHUR)	0	9.8	9.4	9.8	7.1	5.2	9.1
$100 \times \varepsilon^{142}Nd$ (versus ordinary chondrites) (ppm)	0 ppm	18 ± 5 ppm	18 ± 5 ppm	18 ± 5 ppm	18 ppm	13 ppm	23 ppm
$^{87}Sr/^{86}Sr$	0.7047	0.70263	0.70260	0.70263	0.7030	0.7034	0.7026
$^{87}Rb/^{86}Sr$	0.085	0.0188	0.0260	0.0260	0.0609	0.0669	0.0549
Rb/Sr	0.029	0.0065	0.0090	0.0090	0.0211	0.0231	0.0190
$^{176}Hf/^{177}Hf$	0.282786	0.28326	0.28330	0.28326	0.28314	0.28305	0.28323
$^{176}Lu/^{177}Hf$	0.0336	0.0524	0.0450	0.0406	0.0377	0.0367	0.0387
Lu/Hf	0.237	0.369	0.317	0.286	0.266	0.259	0.273
$\varepsilon^{176}Hf$ (versus CHUR)	0	16.8	16.2	16.8	12.6	9.5	15.8

[a]CHUR is Chondrite Uniform Reservoir. Many of the values for the nonchondritic BSE in this table are adopted from *Caro and Bourdon's* [2010] estimates for SCHEM or are similar to their values. The $^{143}Nd/^{144}Nd$ and $^{176}Hf/^{177}Hf$ values for CHUR are from *Bouvier et al*. [2008], where the CHUR $^{143}Nd/^{144}Nd$ value is similar to the *Jacobsen and Wasserburg* [1980b] value. DMM compositions are from *Workman and Hart* [2005] (WH05), *Salters and Stracke* [2004] (SS04), and *Boyet and Carlson* [2006] (BC06). Following *Caro and Bourdon* [2010], the $\varepsilon^{176}Hf$ of the nonchondritic BSE is calculated from its $\varepsilon^{143}Nd$ by using the equation for the mantle array from *Chauvel et al*. [2008]: $\varepsilon^{176}Hf = 1.59^{*}\varepsilon^{143}Nd + 1.28$. The table also provides enriched and depleted bounds about an average nonchondritic BSE composition. These enriched and depleted estimates are generated from the uncertainty on the difference in $^{142}Nd/^{144}Nd$ (and hence difference in Sm/Nd) between Earth and O-chondrites.

mantle, and the ratios are relatively constant in oceanic lavas: Sm/Hf [*Chauvel and Blichert-Toft*, 2001], Sr/Nd [*Sun and McDonough*, 1989], La/Th [*Willbold and Stracke*, 2006], Ba/Rb [*Hofmann and White*, 1983], Ba/Th [*Salters and Stracke*, 2004], Nb/U [e.g., *Hofmann et al*., 1986], and K/U [e.g., *Jochum et al*., 1983]. We use the trace element compilation on ocean island basalts (OIBs) from *Willbold and Stracke* [2006] to determine average trace element ratios and their associated uncertainty, and we exclude lavas with <10 wt% MgO to avoid fractionation of the trace element ratios during magmatic evolution (Table 2). High$^{3He/4He}$ ratios are associated with OIB and not with MORB, so a trace element compilation based on OIB [*Willbold and Stracke*, 2006] (Table 2) is used to define the spidergram of the high $^{3}He/^{4}He$ mantle that is here assumed to reflect the nonchondritic BSE. Additionally, the canonical ratios that we employ are broadly similar in all OIB, and should therefore also reflect the ratios in the subset of OIB with high $^{3}He/^{4}He$ (and thus the ratios in the nonchondritic BSE). Therefore, using trace element ratios in OIBs from Table 2, the Sr/Nd ratio (15.3) can be used to link the Rb-Sr and Sm-Nd sections of the spidergram for the high $^{3}He/^{4}He$ mantle, and the Sm/Hf ratio (1.44) links the Sm-Nd and Lu-Hf sections, thereby providing the "backbone" of the nonchondritic BSE spidergram from Rb to Lu (Figure 2).

2.3. Relative Abundances of Rare Earth Elements (REEs) and Elements (Y, Zr, and Ti) Bracketed by REEs

[14] Using isotopic constraints and canonical trace element ratios, the relative abundances of just three of the REEs, Sm, Nd, and Lu, are estimated for the nonchondritic BSE (section 2.2), but the relative abundances of the remaining 11 naturally occurring REE's are not known. One way to extrapolate the abundances of the remaining REEs is to fit a second-order polynomial through the normalized abundances of Nd, Sm, and Lu (Figure 3).

[15] However, the fit in Figure 3 provides no constraints on the shape of the REE spidergram for the elements more incompatible than Nd: La, Ce and Pr. In order to estimate this part of the spidergram we first identify terrestrial peridotite samples with Sm/Nd (0.344) and Lu/Nd (0.0634) ratios, ratios of the three REEs determined using isotopic constraints, that approach the ratios calculated for nonchondritic BSE calculated in Table 3. Next, we compare the normalized median REE values from this subset of peridotite samples with the polynomial fit through Sm, Nd and Lu to evaluate whether the La, Ce, and Pr in our model spidergram are qualitatively similar for these elements in peridotites.

[16] We select the subset of peridotites from the MS95 database that have Sm/Nd (0.344 ± 0.034) and Lu/Nd (0.0634 ± 0.0190) ratios most similar to the values for nonchondritic BSE (Table 3). A larger or smaller range of Sm/Nd and Lu/Nd values could be permitted, but the selected range provides a reasonable number ($n = 20$) of peridotites. From this set of 20 peridotites, we exclude peridotites enriched in incompatible elements by metasomatic processes. Peridotites with $(La/Yb)_N > 2$ [*Lyubetskaya and Korenaga*, 2007] or peridotite with high La/Ce [$(La/Ce)_{Nz} = 1.25$] (where N signifies normalization to the chondrite-based BSE composition from MS95) are removed, leaving 18 peridotites for consideration. There are only seven REEs that have been analyzed in all 18 peridotites. The shape of the REE spidergram formed by the median normalized concentrations of the seven REEs in the 18 peridotites is in good agreement with the relative abundances of Sm, Nd and Lu for the nonchondritic BSE REE spidergram in Figure 3 (the absolute abundances are different, but the relative abundances are similar). Critically, the relative normalized abundances of the three REEs extrapolated from the polynomial, La and Ce, also agree with the relative normalized median values for La and Ce obtained from the peridotites. Therefore, we apply the polynomial fit through Sm, Nd, and Lu to extrapolate the compositions of

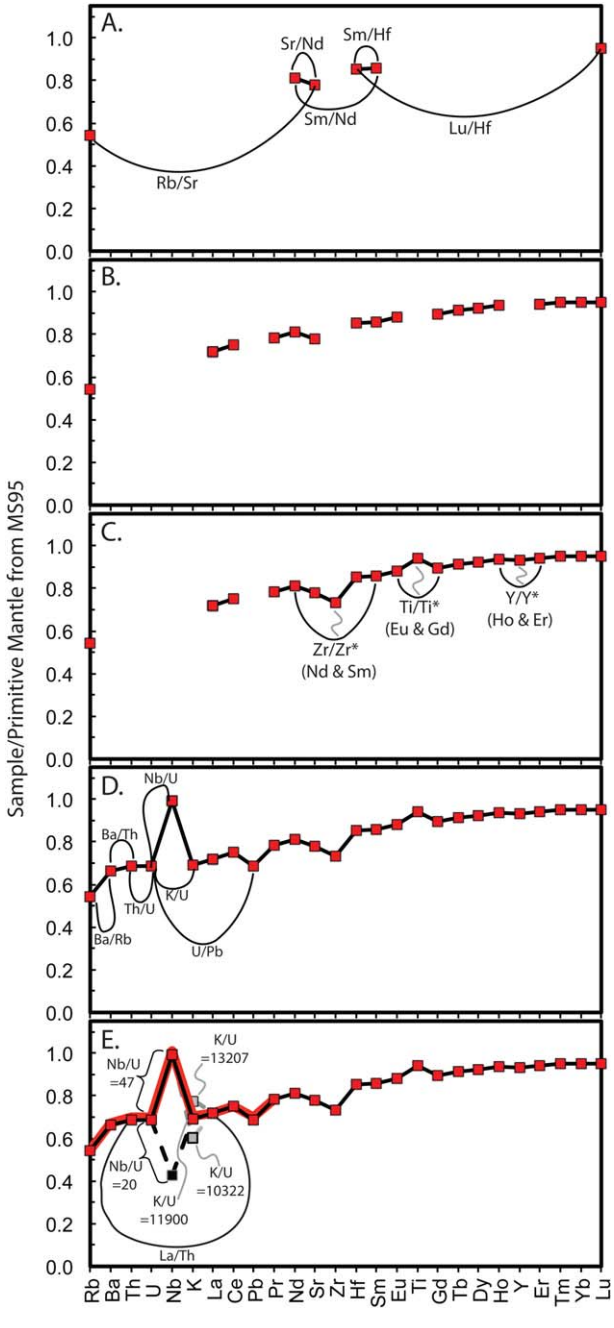

Figure 2. Constructing the spidergram for the nonchondritic BSE presented in Table 3, which is anchored to a Lu concentration intermediate between that of DMM and a chondrite-based BSE. (a) Parent-daughter ratios are calculated to generate nonchondritic BSE $^{87}Sr/^{86}Sr$, $^{143}Nd/^{144}Nd$, and $^{176}Hf/^{177}Hf$ (see Figure 1) ratios in a closed-system model over the age of the Earth. The resulting ratios are used to generate three sections of the spidergram (Rb-Sr, Sm-Nd, Lu-Hf; using the ratios from Table 1) that are linked together using canonical ratios in OIBs (Sr/Nd and Sm/Hf; Table 2). Thus, the "backbone" of the spidergram is constrained from Rb to Lu (see sections 2.1 and 2.2 for details). (b) While the relative abundances of three REEs are calculated using isotopic constraints (Sm, Nd, and Lu), the relative abundances of the other 11 naturally occurring REEs are estimated using different methods (see section 2.3 of text and Figure 3 for details). (c) Three elements that have mineral-melt partition coefficients bracketed by the REEs—Zr, Ti, Y—are added by using their calculated anomalies in OIBs (Zr/Zr^*, Ti/Ti^*, Y/Y^*; see Table 2 and section 2.3). Note that there is no resolvable Eu-anomaly [where $Eu/Eu^* = Eu_N/\sqrt{(Sm_N \cdot Gd_N)}$] in the OIB composition constructed from the least evolved lavas (i.e., MgO > 10 wt%), and we use Eu and Gd to bracket Ti in order to calculate Ti/Ti^* (see section 2.3 and Table 2). (d) The radioactive heat producing elements (Th, U, K), Pb, and other highly incompatible elements (Ba, Nb) are added to the spidergram using isotopic constraints (Th/U, U/Pb) and canonical ratios (K/U, Nb/U, Ba/Rb, Ba/Th). See section 2.4 for details. (e) Possible modifications to the nonchondritic BSE spidergram. The composition resulting from an alternative method for integrating Th, U, K, Pb, Ba, and Nb into the spidergram, from "right to left" (see section 2.4 for details), is shown with the heavy red line from Rb to Pr, which is quite similar to the composition in Figure 2d. This alternative method uses the canonical Th/La ratio. The relative abundance for Nb is shown for a low Nb/U ratio (20; black square) and for a high Nb/U ratio (47; red square). The affect of a higher K/U ratio (13,207) and a lower K/U ratio (10,322) is also shown with gray squares; the preferred K/U ratio (11,900) is shown as a red square. Primitive mantle is from MS95.

Table 2. Trace Element Ratios in Global OIBs Used to Construct the Nonchondritic BSE Mantle Source for high $^3He/^4He$ lavas[a]

	Mean (All MgO)	±1σ (Standard Deviation, %)	*n*	Mean (MgO > 10 wt%)	±1σ (Standard Deviation, %)	*n*
Sm/Hf	1.47	16	163	1.44	20	56
Sr/Nd	15.1	20	243	15.3	23	74
La/Th	8.5	18	201	8.4	15	64
Ba/Th	76.6	36	228	80.2	40	71
Ba/Rb	13.0	31	301	13.4	38	83
Ba/Rb (WH83)	12.45	10	17	na	na	na
Nb/U	46.8	26	158	50.8	28	46
Nb/U (OIB-H03)	52	na	na	na	na	na
Ce/Pb	25.1	8	135	23.9	37	40
Ti/Ti* (Gd, Eu)	1.02	14	124	1.06	15	41
Y/Y* (Ho, Er)	1.03	10	104	0.99	8	37
Zr/Zr* (Sm, Nd)	0.91	14	183	0.90	14	63
Eu/Eu* (Sm, Gd)	1.04	5	124	1.03	4	41
K/U	10,322	42	150	10436	51	47
K/U (OIB-A09)	11,900	9	87	na	na	na
K/U (MORB-AO9)	19,000	7	87	na	na	na
K/U (MORB-G13)	13,207	4	1000's[b]	na	na	na

[a]WH83 = *Hofmann and White* [1983], A09= *Arevalo et al*. [2009], H05 = *Hofmann* [2003], G13 = *Gale et al*. [2013]. Unless indicated otherwise, all canonical ratios are calculated using OIB data compiled in *Willbold and Stracke* [2006]. Average values are provided for the entire OIB data set from *Willbold and Stracke* [2006] and for the subset of samples that have >10 wt% MgO (to ensure that extensive crystal fractionation does not modify the trace element ratios). The subset of trace element data from OIBs with MgO > 10 wt% are used in Table 3. Two estimates for K/U from *Arevalo et al*. [2009] are given, one for OIB and the other for MORB. The elements used to bracket the calculated elemental anomalies (Ti/Ti*, Y/Y*, Zr/Zr*, Eu/Eu*) are provided in parenthesis.

[b]This is an average of samples from 269 ridge segments; thousands of samples were used to calculate the ridge-segment mean values.

Table 3. Trace Element Composition of the Nonchondritic BSE, Which Also Represents the High $^3He/^4He$ Mantle Composition[a]

	Chondritic Earth [MS95] (ppm)	DMM [WH05] (ppm)	DMM [SS04] (ppm)	DMM [BC06] (ppm)	Nonchondritic BSE: High $^3He/^4He$ Mantle Average (This Study) (ppm)	Nonchondritic BSE: High $^3He/^4He$ Mantle Upper Limit (This Study) (ppm)	Nonchondritic BSE: High $^3He/^4He$ Mantle Lower Limit (This Study) (ppm)
Rb	0.6	0.05	0.088	0.10	0.33	0.39	0.27
Ba	6.6	0.563	1.2	1.37	4.4	5.3	3.6
Th	0.0795	0.0079	0.0137	0.016	0.055	0.066	0.045
U	0.0203	0.0032	0.0047	0.0054	0.014	0.017	0.011
Nb	0.658	0.1485	0.21	0.24	0.65	0.79	0.53
K	240	49.8	60	68.4	166	201	136
La	0.648	0.192	0.234	0.26	0.47	0.53	0.41
Ce	1.675	0.55	0.772	0.87	1.26	1.42	1.12
Pb	0.15	0.018	0.0232	0.035	0.10	0.12	0.08
Pr	0.254	0.107	0.131	na	0.20	0.22	0.18
Nd	1.25	0.581	0.713	0.81	1.01	1.12	0.92
Sr	19.9	7.664	9.8	11.1	15.5	17.1	14.0
Zr	10.5	5.082	7.94	na	7.7	8.4	7.0
Hf	0.283	0.157	0.199	0.22	0.24	0.26	0.22
Sm	0.406	0.239	0.27	0.29	0.35	0.38	0.32
Eu	0.154	0.096	0.107	0.12	0.14	0.15	0.13
Ti	1205	716.3	798	na	1134	1217	1052
Gd	0.544	0.358	0.395	0.42	0.49	0.52	0.45
Tb	0.099	0.07	0.075	na	0.090	0.096	0.084
Dy	0.674	0.505	0.531	0.58	0.62	0.66	0.58
Ho	0.149	0.115	0.122	na	0.14	0.15	0.13
Y	4.3	3.328	4.07	na	4.0	4.2	3.8
Er	0.438	0.348	0.371	0.39	0.41	0.44	0.39
Tm	0.068	na	0.06	na	0.064	0.068	0.061
Yb	0.441	0.365	0.401	0.40	0.42	0.44	0.40
Lu	0.068	0.058	0.063	0.063	0.064	0.068	0.061

[a]The upper and lower limits on the nonchondritic BSE (high $^3He/^4He$ mantle) composition are calculated by taking into account two separate sources of uncertainty: (1) The uncertainty on the Lu concentration, which anchors the nonchondritic BSE spidergram, is ±5.5%, and this uncertainty is propagated through the entire spidergram, (2) The range in isotopic compositions for the nonchondritic BSE (given in Table 1) give rise to a range in parent-daughter ratios (the upper limit uses the "enriched" nonchondritic BSE values from Table 1, and the lower limit uses the "depleted" nonchondritic BSE values). Note that the canonical ratios from Table 2 are not varied when calculating the upper and lower compositional limits. The K and Ti concentrations are calculated independently of the concentrations shown in Table 4.

the other 11 naturally occurring REE's, including La, Ce and Pr, to obtain a plausible REE spidergram for the nonchondritic BSE (Figure 3). The averaged peridotite spidergram is shown only to demonstrate that the REE pattern for the high $^3He/^4He$ mantle composition is not an impossible pattern in terrestrial rocks, and we emphasize that our new BSE composition does not rely on peridotite compositions.

[17] During melting or solidification Y is partitioned into the melt phase in approximately the same way as most heavy REEs. To estimate the relative abundance of Y, we then assume that it has a normalized abundance intermediate between Ho and Er. We use the OIB database of *Willbold and Stracke* [2006] to calculate the average Y-anomaly, or Y/Y^* [where $Y/Y^* = Y_N/\sqrt{(Ho_N \cdot Er_N)}$] for the least evolved lavas and obtain a mean Y/Y^* value of 1.03 (Table 2) (Figure 2).

[18] We use a similar method to incorporate Zr and Ti into the nonchondritic BSE spidergram. Zr/Zr^* [$Zr/Zr^* = Y_N/\sqrt{(Sm_N \cdot Nd_N)}$] is 0.90 in the OIB database (Table 2). We place Zr between Sm and Nd so that Zr in the spidergram has a Zr/Zr^* value of 0.90 (Figure 2). The relative abundance of Ti in the nonchondritic BSE spidergram is given by Ti/Ti^* [where $Ti/Ti^* = Ti_N/\sqrt{(Gd_N \cdot Eu_N)}$], which is 1.06 in the OIB database (Figure 2 and Table 2). By excluding lavas with MgO < 10 wt%, we avoid effects related to Eu fractionation in the filtered data set (Table 2).

2.4. Filling in the Backbone of the Nonchondritic BSE: The Highly Incompatible Elements—U, Th, K, Ba, Nb—and Pb

[19] The most highly incompatible elements, the elements with compatibilities between Rb and La, and Pb (which has a compatibility between Ce and Nd) [*Hofmann*, 2003], still remain to be incorporated into the nonchondritic BSE spidergram. These elements are integrated into the spidergram using canonical (Ba/Rb, Nb/U, K/U, La/Th, Ba/Th) and isotopically constrained (Th/U, U/Pb) ratios.

[20] We suggest two similar approaches for estimating the abundances of U, Th, K, Pb, Ba, Nb and Pb in the nonchondritic BSE spidergram. The first integrates these elements into the spidergram sequentially from "left to right," starting with Rb, which is already included in the backbone of the spidergram in section 2.2, and continuing to the less incompatible trace elements. Using the canonical Ba/Rb ratio in OIBs (13.4; Table 2), Ba is added to the right of Rb on the spidergram. Ba/Th is approximately constant in oceanic lavas [e.g., *Willbold and Stracke*, 2006], with a value of 80.2 (Table 2), and this ratio permits insertion of Th to the right of Ba on the spidergram (Figure 2).

[21] We then calculate the relative abundance of U by pairing Th with the estimated Th/U ratio (3.9) of the nonchondritic BSE (Figure 2), which is required to generate the Pb-isotopic composition of much of the global OIB array, including high $^3He/^4He$ lavas, on a 4.50 Ga geochron [*Jackson et al.*, 2010].

[22] We estimate the U/Pb ratio from isotopic constraints, and combine this ratio with our estimate for the relative abundance of U to insert Pb into the nonchondritic BSE spidergram. We select a $^{238}U/^{204}Pb$ ($\mu = 8.5$) ratio that places the nonchondritic BSE on a 4.5 Ga geochron where it intersects the OIB array in $^{207}Pb/^{204}Pb$ versus $^{206}Pb/^{204}Pb$ isotopic space. The U/Pb ratio (~0.136; Figure 2) is the same as used by MS95. Although often considered to be a canonical ratio, we do not use the Ce/Pb ratio is OIBs to constrain the relative Pb abundance in the nonchondritic BSE. The Ce/Pb ratio in the spidergram (~12; Table 3) is approximately half the canonical ratio in OIBs (~25) [*Hofmann et al.*, 1986]. Because it is chalcophile, Pb can be strongly influenced by the presence of sulfides in the mantle source, and as a result the Ce/Pb ratio of the mantle source of high $^3He/^4He$ OIBs (here argued to be ~12) may differ from the melt (~25) [*Hart and Gaetani*, 2006].

[23] In addition to Pb, two other elements, K and Nb, are anchored to U in the spidergram (Figure 2). To constrain the relative abundance of Nb we use the canonical Nb/U ratio observed in OIBs, which is about 46.8–50.8 (Table 2), and is similar to *Hofmann's* [2003] value of 52 for "nonenriched mantle-type" samples. These Nb/U ratios generate a positive Nb anomaly in the nonchondritic BSE spidergram, which is consistent with earlier observations of "nonenriched mantle-type" OIBs in general and Nb-enrichment in high $^3He/^4He$ OIBs in particular [*Jackson et al.*, 2008].

[24] The canonical K/U ratio is used to incorporate K by anchoring its value to U (Figure 2). The K/U ratio is relatively constant in oceanic lavas [e.g., *Wasserburg et al.*, 1964; *Arevalo et al.*, 2009] and continental crust [*Jochum et al.*, 1983; *Palme and O'Neil*, 2003; *Lyubetskaya and Korenaga*, 2007], and this ratio therefore reflects the composition of

BSE. We adopt the most recent K/U estimate (11,900) for OIBs [*Arevalo et al*., 2009], which is somewhat higher than the average OIB K/U value of 10,322 from *Willbold and Stracke* [2006] (Table 2). However, there appears to be variability in the oceanic mantle, as suggested by the K/U ratio of 19,000 proposed for the MORB mantle [*Arevalo et al*., 2009]. We note that the value of 19,000 is significantly higher than a recent estimate for the K/U of the MORB mantle of 13,207 [*Gale et al*., 2013], and we adopt the lower K/U ratio for MORB, which is based on a much larger data set, as the upper limit for the K/U of the oceanic mantle. The lower limit is given by the K/U ratio (10,322) from the *Willbold and Stracke* [2006] data set (Table 2). As a check for the internal consistency of the K/U ratio in the spidergram, we note that the K/U ratio of 11,900 results in a K/La ratio for the nonchondritic BSE of 357 (Table 3), which is within the range of accepted values for the canonical K/La ratio (330 ± 30) in oceanic lavas that is though to reflect the mantle source ratio [*O'Neill and Palme*, 1998; *Palme and O'Neil*, 2003; *Lyubetskaya and Korenaga*, 2007].

[25] It is difficult to assess the uncertainty associated with the relative abundances of the most incompabile elements in the nonchondritic BSE spidergram (see section 3). However, the internal consistency of our method can be examined by employing a different trace element ratio to construct this portion of the spidergram (Figure 2). Having integrated the most incompatible elements from "left to right," we suggest a second, complementary method that integrates the most incompatible elements from "right to left" and utilizes a different ratio, La/Th, that is relatively constant in OIBs (La/Th = 8.4 ± 1.2, 1σ standard deviation of the mean; Table 2) and thought to reflect the ratio in the OIB mantle [*Willbold and Stracke*, 2006]. The La/Th ratio bridges the section of the spidergram from the light REEs to Th. The Ba/Th ratio (80.2) provides the relative abundance of Ba. Rb is already included in the backbone of the spidergram (section 2.2), and a Ba/Rb ratio does not need to be estimated to incorporate Rb. Instead, the Ba/Rb ratio that results from this alternative "right to left" method (13.6) can be used to evaluate the internal consistency of our overall approach for estimating the abundances of the most incompatible elements from "right to left," and is similar to the average OIB Ba/Rb ratio of 13.4 in Table 2. The remaining highly incompatible elements are integrated into the nonchondritic BSE spidergram using the same ratios and assumptions as above: U (from Th/U), Pb (U/Pb), Nb (Nb/U), and K (K/U). The resulting K/La value for the nonchondritic BSE (363) is similar to the range of accepted K/La values (330 ± 30) in oceanic lavas. This right-to-left spidergram construction yields a pattern that is quite similar to the spidergram architecture generated by construction from left-to-right (Figure 2, Panel E).

2.5. Anchoring the Nonchondritic BSE Spidergram to Lutetium (Lu)

[26] Whereas the overall shape of the spidergram for the nonchondritic BSE can be constructed using isotopically constrained parent-daughter ratios and canonical trace element ratios (sections 2.2 through 2.4), the absolute abundances of the trace elements are not known. To this end, we estimate the concentration of the least incompatible element in the nonchondritic BSE spidergram, Lu, to "anchor" the spidergram such that absolute concentrations of the other trace elements in the spidergram can be determined. There is little difference between the abundance of Lu in DMM (0.058–0.063 ppm) [*Salters and Stracke*, 2004; *Workman and Hart*, 2005] and chondrite-based estimates for BSE (0.0675 ppm; MS95), and we argue below that the abundance of Lu in a nonchondritic BSE is bracketed by its abundance in DMM and the chondrite-based BSE.

[27] Lu is incompatible during melting. Therefore, if the nonchondritic BSE acquired its superchondritic Sm/Nd ratio and incompatible element depletion by extraction of early enriched crust from an originally chondrite-based BSE similar to MS95, then the abundance of Lu in a nonchondritic BSE must be lower than its abundance in chondrite-based estimates for BSE. On the other hand, DMM has experienced greater melt depletion than the nonchondritic BSE, as evidenced by the combination of higher Sm/Nd ratios and $^{143}Nd/^{144}Nd$ ratios in DMM (Table 1). Therefore, the nonchondritic BSE must have higher Lu abundances than DMM. For the nonchondritic BSE, we adopt a Lu concentration of 0.064 ppm (Table 3), which is the average of Lu concentration estimates for the chondrite-based BSE composition from MS95 and estimates of DMM (using an average of the Lu concentrations from *Workman and Hart* [2005] and *Salters and Stracke* [2004]). In this way, the Lu concentration of the nonchondritic BSE is tightly bracketed, and is within 5.5% of the Lu concentrations of the upper bound (i.e., the chondrite-based BSE) or the lower bound (DMM).

[28] We note that, in contrast to our approach of anchoring the new BSE composition to Lu, *O'Neill and Palme* [2008] anchor their nonchondritic BSE composition to a K abundance that provides a possible solution to the missing Ar paradox. Their approach results in highly incompatible elements being ~50% lower than MS95 values, while our approach yields values that are only ~30% lower. We consider the estimate for K concentration in a nonchondritic BSE to be more fraught with error than the estimate for Lu, and we argue that Lu offers a more robust anchor for the trace element concentrations of a nonchondritic BSE.

2.6. Bracketing the Major Element Composition of a Nonchondritic BSE

[29] In the same way that the Lu concentration of a nonchondritic BSE should not be lower than the Lu concentration in DMM, or higher than the Lu concentration in a chondrite-based BSE composition, the major element composition of the nonchondritic BSE must also be bracketed by DMM and a chondrite-based BSE. Compatible elements, such as Mg, will have lower concentrations in nonchondritic BSE than in DMM, but higher concentrations than in a chondrite-base BSE. Incompatible elements, such as K, will have higher concentrations in the nonchondritic BSE than in DMM, but lower concentration than in a chondrite-based BSE. For most of the major elements, there is little variability between estimates for the major element composition of DMM and chondrite-based estimates for BSE. This owes to the fact that relatively little melt (from 1.5–2% [*Salters and Stracke*, 2004] to 2–3% [*Workman and Hart*, 2005]) is extracted from a chondrite-based BSE to generate DMM. (Even less melt would be extracted from a chondrite-based BSE to generate the nonchondritic BSE). Such a small amount of melt extraction has only a minor affect on the abundances of most major elements (which are either compatible or slightly incompatible) in the residual peridotite, excluding K, which is highly incompatible. Therefore, a simple average of the major element abundances in DMM and BSE is sufficient to bracket the major element abundances of the nonchondritic Earth, particularly for the compatible or moderately incompatible elements, where the difference in the abundance of an element between DMM and BSE is generally small (Table 4). For example, the SiO_2 concentration of the chondrite-based BSE is 45.0 wt% and the average concentration of SiO_2 in DMM is 44.8 wt% (Table 4) are quite similar, so the SiO_2 abundance of the nonchondritic BSE is tightly bracketed at $44.9 \pm 0.1\%$. The goal of this study is to provide a first-order estimate that brackets the major element composition of the

Table 4. Bracketing the Major Element Composition of a Nonchondritic BSE, Which Represents the High $^3He/^4He$ Mantle[a]

	Chondritic Earth [MS95] (wt%)	DMM [WH05] (wt%)	DMM [SS04] (wt%)	Nonchondritic BSE High $^3He/^4He$ Mantle (This study) (wt%)		Bracketing Range (wt%)
SiO_2	45.0	44.7	44.9	44.9	±	0.1
Al_2O_3	4.45	3.98	4.28	4.29	±	0.16
FeO	8.05	8.18	8.07	8.09	±	0.04
MnO	0.135	0.13	0.135	0.13	±	0.001
MgO	37.8	38.73	38.22	38.14	±	0.34
CaO	3.55	3.17	3.5	3.44	±	0.11
Na_2O	0.36	0.13 (0.28)	0.29	0.28 (0.32)	±	0.07 (0.04)
Cr_2O_3	0.384	0.57	0.37	0.43	±	0.04
NiO	0.25	0.24	0.249	0.25	±	0.003
TiO_2	0.201	0.13	0.133	0.17	±	0.03
K_2O	0.029	0.006	0.007	0.018	±	0.011
P_2O_5	0.021	0.019	0.009	0.018	±	0.003
Mg#	89.3	89.4	89.4	89.4	±	0.04

[a]The concentration of a major element in the nonchondritic BSE is estimated to lie between the average concentration of a given element in chondrite-based compositional estimates for BSE [e.g., *McDonough and Sun*, 1995] and DMM (where DMM is the average of the compositions from *Workman and Hart* [2005] and *Salters and Stracke* [2004]). See section 2.6 of the text for explanation. For a given element, the average concentration of the chondrite-based BSE and DMM concentratios is taken to be the concentration for the nonchondritic BSE. The uncertainty on a given elemental concentration is simply the absolute difference between the concentration in the nonchondritic BSE and the two bracketing reservoirs, DMM and the chondrite-based BSE. *Workman and Hart* [2005] provided two estimates for the Na_2O concentratio in DMM. The estimate that more closely matches the Na_2O concentraion in *Salters and Stracke* [2004] is shown in parenthesis. Concentrations of Ti and K in this table are 1000 ± 200 and 150 ± 90 ppm, respectively. The Ti and K values shown in this table (using methods outlined in section 2.6 of the text) are calculated independently of the values shown in Table 3 (which uses methods outlined in sections 2.1 through 2.5 of the text). Within uncertainty, the two estimates for Ti and K in the nonchondritic BSE agree. Mg# = molar ratio of MgO/(MgO + FeO) * 100.

nonchondritic BSE, and future work may permit a more precise estimate.

[30] Major (Table 4) and trace (Table 3) element concentrations in the nonchondritic BSE are calculated using independent methods. As a check for internal consistency between the independently calculated major and trace elements, we employ a known relationship between CaO (wt.%) and Lu (ppm) concentrations in peridotites, where $Lu = 0.0172 \times CaO + 0.0032$ [*Salters and Stracke*, 2004]. Using the Lu concentration in the nonchondritic BSE of 0.064 ppm (section 2.5 and Table 3), the calculated CaO abundance in is 3.53 wt%, which lies within the uncertainty of the nonchondritic BSE CaO abundance (3.44 ± 0.11 wt%) in Table 4. Additionally, we present independently determined estimates for K and Ti for the nonchondritic BSE in Table 3 (166 and 1118 ppm, respectively) and Table 4 (150 ± 90 and 1000 ± 200 ppm, respectively). We note that, within uncertainties, the two independent estimates for the K and Ti abundances are in agreement. We consider the estimate for K and Ti in Table 3 to be more robust, as the estimate in Table 4 is based on simple bracketing arguments, but we emphasize that all estimates for the K abundance in the Earth are highly uncertain. Nonetheless, these observations demonstrate broad internal consistency between our independent methods for estimating for major and trace element abundances in the nonchondritic BSE.

3. Estimating Uncertainty in the Nonchondritic BSE Composition

[31] *Salters and Stracke* [2004] constructed a trace element source for DMM using a similar approach of "cascading" elemental ratios that we use to calculate the nonchondritic BSE, and they discussed the difficulties associated with estimating uncertainties for each of the elements. They noted that, owing to the use of canonical and isotopically constrained ratios to construct a mantle source, the concentrations of each trace element is linked to the abundances of other elements, and so must be the uncertainties. For example, the Sm abundance is linked to the estimated Lu abundance through a canonical ratio (Sm/Hf) and an isotopically constrained ratio (Lu/Hf). The Sm/Hf ratio has a 1σ deviation of 20% (Table 2). In addition to being dependent on uncertainties associated with the Sm/Hf ratio, the possible range of concentrations for Sm in the nonchondritic BSE is also tied to the uncertainty in Lu/Hf (±2.6%), and to the uncertainty in Lu (±5.5%). To estimate the uncertainties in the concentrations of Sm, or any other trace element, the uncertainties that accumulate with each canonical or isotopically constrained ratio "upstream" of Sm must be added.

[32] *Salters and Stracke* [2004] did not propagate uncertainties in their DMM estimate. Instead, they provided a mantle source estimate that they considered to be "most reasonable" that is based on mean trace element ratios and follows a clear set of criteria that can be tested. They provided a Microsoft Excel™ worksheet that provides full access to the relationships used to calculate the elemental concentrations. Following this precedent, we also provide a Microsoft Excel worksheet (Table S1, supporting information)[1] that allows the reader to follow our calculations in a step-by-step manner. With this spreadsheet, the reader can evaluate the sensitivity of the nonchondritic BSE to different trace element ratios and evaluate how changing a particular ratio will impact the concentrations of other "dependent" elements downstream.

[33] We provide estimates for the upper and lower limits of the nonchondritic BSE spidergram in Table 3. Uncertainties in the isotopically constrained parent daughter ratios (owing to uncertainty in the Sr, Nd, and Hf isotopic compositions; see sections 2.1 and 2.2) and Lu concentrations (see section 2.5) for the nonchondritic BSE are propagated to generate the range of compositions shown. The compositional range for the nonchondritic BSE is illustrated in Figure 4, and the average and upper and lower limits on the new BSE composition are provided in Table 3.

4. Melting the Nonchondritic BSE Composition to Make High ^{3}He/^{4}He Lavas

[34] *Jackson et al*. [2010] suggested that the highest ^{3}He/^{4}He lavas erupted globally (up to 50 Ra, ratio to atmospheric), from the Baffin Island flood basalt [*Stuart et al*., 2003; *Starkey et al*., 2009], are melts of an early-formed depleted mantle reservoir with high ^{3}He/^{4}He, which we argue represents the lithophile element composition of a nonchondritic BSE. We explore whether melts of the nonchondritic BSE calculated here (Table 3) can yield trace element patterns that resemble the highest ^{3}He/^{4}He lavas from Baffin Island. We

[1]Additional supporting information may be found in the online version of this article.

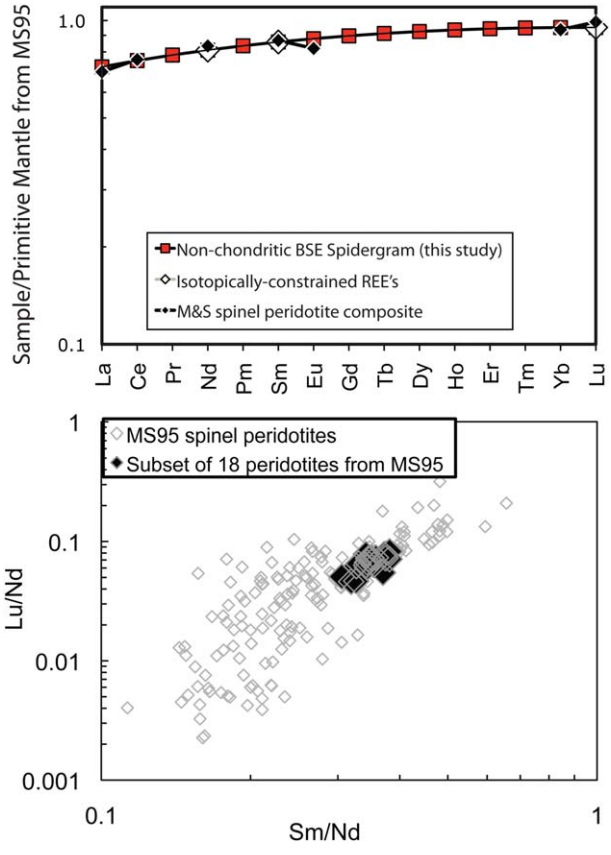

Figure 3. Determining the shape of the REE spidergram for a nonchondritic BSE. (top) A degree-two polynomial fit through the isotopically constrained REEs (white diamonds: Sm, Nd, and Lu) is used to reconstruct the relative values of the other 11 naturally occurring REEs (Pm is extinct, but is included for the polynomial fit). The fit shown in the figure is for the average nonchondritic BSE composition in Tables 1 and 3: $y = -0.00124 \cdot x^2 + 0.0365 \cdot x + 0.684$, where x is the integer value of the REE, with increasing mass from La (1) to Lu (15), and y is the primitive mantle normalized abundance of a given REE. (bottom) Spinel peridotites from the MS95 peridotite database. We allow Sm/Nd and Lu/Nd of the selected peridotites to vary within 10% and 30%, respectively, of the nonchondritic BSE composition to obtain a reasonably large number of peridotites for comparison to this composition. Lu/Nd shows nearly 30 times more variability than Sm/Nd, and a larger variance for the former ratio is permitted when filtering the peridotite samples. A subset of 18 samples have been selected because they have Sm/Nd and Lu/Nd ratios similar to our estimate for a nonchondritic BSE and do not exhibit evidence for metasomatic enrichment (see section 2.3 of text). The normalized median values for the REE abundances from the 18 samples from the MS95 peridotite database are shown (upper panel, black diamonds). The peridotite-based spidergram has a shape that is broadly similar to the polynomial fit; the peridotite spidergram has been "DC-shifted" by a factor of 1.35 so that it overlaps with the polynomial fit. Note that the natural peridotite spidergram is included in the figure to assess the shape of the model spidergram, not its absolute abundances. See section 2.3 for details. Primitive mantle is from MS95.

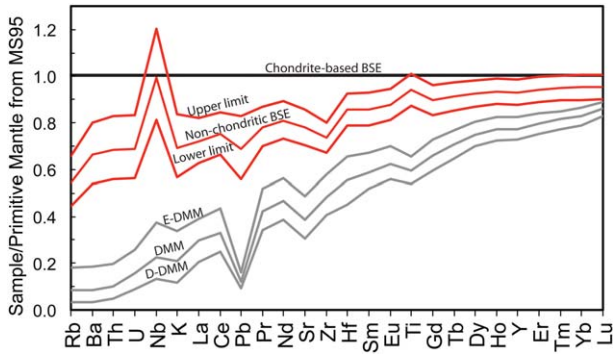

Figure 4. Spidergram for the nonchondritic BSE with upper and lower bounds (from Table 3). The gray lines represent DMM, E-DMM, and D-DMM, and are from *Workman and Hart* [2005]. Primitive mantle is from MS95.

select the highest $^3He/^4He$ lava (DUR8 from *Starkey et al.*, 2009) from Baffin Island and correct the trace element abundances for olivine fractionation by adding equilibrium olivine until the lava is in equilibrium with Fo_{90} olivine (see method in *Jackson et al.* [2010]). This generates an estimate of the trace element composition of the primary melt in equilibrium with the Baffin Island mantle, with the exception of K and Rb, which have been mobilized during weathering [*Jackson et al.*, 2010].

[35] We compare the primary melt trace element composition of DUR8 to two different trace element compositions calculated using simple melting models of the nonchondritic BSE (Table 3). The two calculated melts were generated using two nonmodal aggregated fractional melting models that have different trace element partition coefficients and mineral and melt modes. The melt models are outlined in *Jackson et al.* [2010] (which refers to melt models 1 and 2). Both melting models generate trace element patterns that are similar to the highest $^3He/^4He$ Baffin Island lava when the degree of melting is ~14% (the two melt models require somewhat different contribution from melt in the garnet and spinel stability fields; see Figure 5). This is within the range of melting previously suggested for lavas associate with this large igneous province [*Herzberg and Gazel*, 2009].

[36] Of note is that Rb and K exhibit higher concentrations in the melt models than the olivine fractionation-corrected DUR8 lava, and we attribute this difference to alkali loss from weathering of DUR8 [*Jackson et al.*, 2010]. In summary, simple melt models of the nonchondritic BSE calculated here broadly reproduce the trace element patterns observed in the highest $^3He/^4He$ Baffin Island lava.

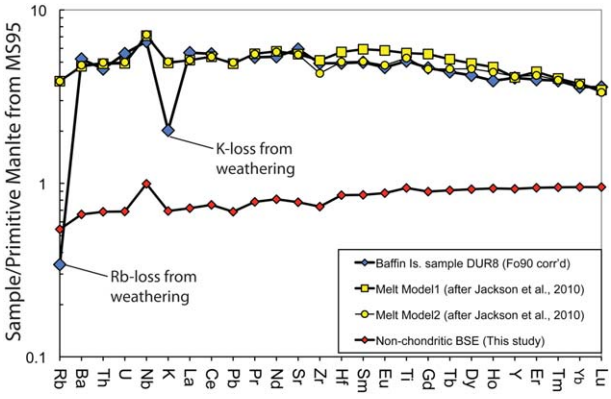

Figure 5. Melting models applied to the nonchondritic BSE (see Table 3) yield calculated melt spidergrams that are similar to the highest ^{3}He/^{4}He lava globally (sample DUR8 from Baffin Island) [*Starkey et al*., 2009]. See section 4 for details. The Baffin lava shown here has been corrected for olivine fractionation to be in equilibrium with Fo90 olivine. Both melt models, model 1 and 2, are described in detail in *Jackson et al*. [2010]. The melting models generate melt compositions similar to the high ^{3}He/^{4}He lava when the degree of melting is 14%. Model 1 requires 50% melting in the garnet stability field (the rest in the spinel stability field), and model 2 requires only 20% melting in the garnet stability field. The nonchondritic BSE (this study, Table 3) is shown for comparison. Many Baffin Island lavas, including DUR8, have lost Rb and K during weathering, and we attribute the offset of these two elements between DUR8 and the melt model compositions to be a result of alkali loss during weathering. There is no evidence for mobilization of other elements (like Ba and U) in this sample. The Pb concentration was not reported for this sample [*Starkey et al*., 2009]. Finally, the Nb/Ta ratio (11.0) suggests no evidence for contamination by W-carbide, and the positive Nb anomaly in DUR8 appears to be a primary magmatic feature inherited from the high ^{3}He/^{4}He Baffin Island mantle source. Primitive mantle is from MS95.

5. Geodynamic Implications for a Nonchondritic BSE

5.1. A Solution to the Earth's "Missing Ar"

[37] ^{40}Ar is the radiogenic decay product of ^{40}K ($T_{1/2} = 1.3$ Ga). The existing ^{40}Ar in the atmosphere and solid Earth is almost entirely a result of ^{40}K decay, and therefore Earth's ^{40}Ar is directly related to the Earth's K abundance. However, the absolute abundance of K is unknown because K is a volatile element that was partly lost from the Earth during accretion (e.g., MS95). Therefore, to constrain the ^{40}Ar budget of the Earth, we must first reliably estimate the K abundance of the Earth.

[38] One way to constrain K is to assume a chondritic U abundance (~20 ppb) and then calculate the K abundance by using the global K/U ratio (~10^4) measured in oceanic basalts (MS95), which is thought to broadly reflect the primitive ratio in the Earth [e.g., *Jochum et al*., 1983; *Allègre et al*., 1996]. Depending on the preferred U concentration and K/U ratio, this approach yields a primitive K abundance in the range 230–270 ppm [*Jochum et al*., 1983; MS95; *Allègre et al*., 1996]. The decay of ^{40}K will, in turn, generate 13–15·10^{16} kg of ^{40}Ar over 4.5 Ga, which is partitioned among Earth's atmosphere, crust, and mantle. The atmosphere has currently 6.6·10^{16} kg ^{40}Ar [*Turekian*, 1959], or about one half the mass expected from a chondrite-based BSE. The continental crust and depleted mantle are unlikely to host more than a small fraction of the other half [*Allègre et al*., 1996]. Thus, about one half of the expected ^{40}Ar is "missing," a feature which defines the so-called "missing" Ar paradox [e.g., *Allègre et al*., 1996].

[39] Assuming a chondrite-based composition for the BSE, one common solution to the missing Ar paradox is to postulate the existence of a "hidden" gas-rich reservoir in the deep mantle that contains the terrestrial Ar not accounted for in shallow geochemical reservoirs. Other solutions for the missing Ar paradox include significant concentrations of Ar and K in the core [*Chabot and Drake*, 1999; *Lodders*, 1995; *Gessmann and Wood*, 2002], or a lower K/U ratio for BSE [*Albarède*, 1998; *Davies*, 1999], possibly as a result of a deep slab reservoir with low K/U [*Lassiter*, 2004], although this idea is contentious [*Arevalo et al*., 2009].

[40] Our nonchondritic BSE composition provides, however, a potentially straightforward way out of this apparent paradox: Earth simply has ~30% less U and K than a typical chondritic model. To test this simple solution we first evaluate the ^{40}Ar budgets of the atmosphere, continental crust and depleted mantle and obtain a lower bound for K in the Earth. (Any "missing" Ar reservoirs in the Earth would increase the total Ar and raise the minimum K in the Earth.) We compare this estimate for the lower bound for K in the Earth to the range of K concentrations suggested for a nonchondritic BSE composition shown in Table 3. If the two estimates for the K agree, then a hidden missing ^{40}Ar reservoir is not required in the Earth. While a missing "hidden" ^{40}Ar reservoir cannot be excluded, it is important to evaluate whether a missing reservoir is needed.

5.1.1. ^{40}Ar in Continental Crust

[41] The amount of ^{40}Ar in the continental crust is a function of its average K abundance, average

age, and degassing rate overtime [*Allègre et al.*, 1996]. Recent estimates for the ^{40}Ar budgets in continental crust range from 0.1–0.9·10^{16} [*Lyubetskaya and Korenaga*, 2007] to 0.5–1.0·10^{16} kg ^{40}Ar [*Allègre et al.*, 1996] and to <0.87·10^{16} kg ^{40}Ar [*Lassiter*, 2004]. We take 0.1·10^{16} kg to be the lower limit of ^{40}Ar in the continental crust, and 1.0·10^{16} kg ^{40}Ar to be the upper limit. While this range is large, it is clear that continental crust is not a significant reservoir for ^{40}Ar [e.g., *Allègre et al.*, 1996].

5.1.2. ^{40}Ar in DMM

[42] The ^{40}Ar content of DMM can be estimated using two independent methods: The flux of ^{40}Ar from ridges, and the K content of DMM [e.g., *Allègre et al.*, 1996]. The ^{40}Ar flux at ridges can be constrained using ridge ^{3}He flux. The ^{3}He flux measured at ridges is ~1.1·10^{3} mol/yr [*Craig et al.*, 1975; *Farley et al.*, 1995]. When combined with the median MORB ^{3}He/^{4}He ratio (8.2 Ra) [*Graham*, 2002] and the ^{4}He/^{40}Ar ratios measured in MORB glasses (1–100) [e.g., *Honda and Patterson*, 1999], the ^{40}Ar flux from ridges is constrained to be 0.039–3.9·10^{6} kg ^{40}Ar/yr. Assuming an oceanic crust production rate of 20 km^{3}/yr (~5.2·10^{13} kg/yr) [*Lassiter*, 2004], and 10% melting and complete extraction for Ar from the mantle during melting, the depleted mantle hosts 0.028–2.8·10^{16} kg ^{40}Ar (assuming a depleted mantle mass of 4.0·10^{24} kg).

[43] This estimate for ^{40}Ar in DMM has very large uncertainties owing to the variability in ^{4}He/^{40}Ar ratios in MORB glasses [*Allègre et al.*, 1996; *Lassiter*, 2004; *Lyubetskaya and Korenaga*, 2007]. However, *Lassiter* [2004] argues that high ^{4}He/^{40}Ar ratios may not accurately reflect the true ratio of the MORB mantle. This is because Ar is less soluble in melt than He, and is likely to be preferentially degassed relative to He during melting, transport and eruption. The negative correlation between ^{4}He/^{40}Ar and ^{40}Ar concentrations in MORB glasses is consistent with this hypothesis [*Sarda and Moreira*, 2001; *Lassiter*, 2004; *Gonnermann and Mukhopadhyay*, 2007]. Therefore, the high ^{4}He/^{40}Ar ratios measured in degassed glasses represent an upper limit for the mantle ratio. However, the relative abundances of the noble gasses in the "popping rock" (^{4}He/^{40}Ar of ~1.5) [*Moreira et al.*, 1998] are thought to be similar to the undegassed ^{4}He/^{40}Ar ratio of MORB, and therefore reflect the depleted mantle ratio. Consistent with this hypothesis, the ^{4}He/^{40}Ar ratio of popping rock is bracketed by the production ratio of ^{4}He/^{40}Ar in DMM (1.5–2.7, assuming K/U from 8000 to 13,000 and Th/U of 2.5 to 4) [see *Lassiter*, 2004]. In summary, the lower limit for the DMM ^{4}He/^{40}Ar ratio, measured on popping rock with a ^{4}He/^{40}Ar ratio of 1.5, yields a ^{40}Ar flux of 2.6·10^{6} kg/yr from the ridge. This yields our preferred abundance of ^{40}Ar in DMM (~2.0·10^{16} kg) derived from the ^{40}Ar ridge flux.

[44] Estimates using the K abundance of DMM provide higher DMM ^{40}Ar abundances. The abundance of K in DMM has been estimated to be 49.8 ppm [*Workman and Hart*, 2005], 60 ppm [*Salters and Stracke*, 2004], and 68.4 ppm [*Boyet and Carlson*, 2006]. The lowest DMM K abundance (49.8 ppm) [*Workman and Hart*, 2005] generates a ^{40}Ar budget of 2.8·10^{16} kg over 4.5 Ga, and the highest DMM K abundance (68.4 ppm) [*Boyet and Carlson*, 2006] yields 3.9·10^{16} kg ^{40}Ar. The *Boyet and Carlson* [2006] DMM estimate is also the only one calculated for a nonchondritic Earth. In summary, we consider the ^{40}Ar abundance in DMM to lie between the 2.0·10^{16} kg, the preferred value obtained from the ^{40}Ar ridge flux, and 3.9·10^{16} kg, the highest ^{40}Ar value obtained from recent estimates of K in DMM from *Boyet and Carlson*, [2006].

5.1.3. Total ^{40}Ar Budget: Atmosphere, Crust, and Mantle

[45] Together, the atmosphere (6.6·10^{16} kg ^{40}Ar), continental crust (0.1–1.0·10^{16} kg ^{40}Ar) and depleted mantle (2.0–3.9·10^{16} kg ^{40}Ar) comprise a minimum ^{40}Ar budget for the Earth that ranges from 8.7 to 11.5·10^{16} kg. If we assume all of the ^{40}Ar was generated by ^{40}K decay over 4.5 Ga, and that little ^{40}Ar was lost from the silicate Earth and atmosphere during this time, the BSE K concentration is estimated to be approximately 155–205 ppm. This range of K abundances estimated from the ^{40}Ar in the atmosphere, crust and mantle overlaps with the range of values for K suggested here for a nonchondritic BSE (Table 3): When paired with a K/U ratio of 11,900, the low U concentration of a nonchondritic BSE (0.011 to 0.017 ppm, Table 3) generates a range of possible BSE K concentrations from 130 to 200 ppm (Table 3). The range of K abundances calculated from the ^{40}Ar budget of the Earth (155–205 ppm) overlap with the range of K abundances that we estimate for a nonchondric BSE (Table 3). In summary, if BSE has a composition like the nonchondritic BSE we propose, a missing ^{40}Ar reservoir is not required to reconcile Earth's Ar mass balance.

5.2. Continental Crust Extraction From a Nonchondritic BSE

[46] A basic test of our nonchondritic BSE model is that its trace element budget must permit

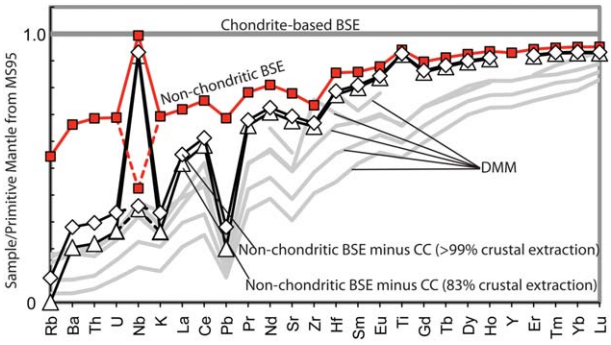

Figure 6. Extracting continental crust from a nonchondritic BSE. For the purposes of the mass-balance model, we use the average nonchondritic BSE composition (red line) from Table 3. In the model, continental crust [from *Rudnick and Gao*, 2003] is extracted from 83% (white triangles) and 99.45% (white diamonds) of a nonchondritic BSE (from Table 3), and continental crust is fixed at 0.555% of BSE's mass [*Galer et al.*, 1989]. Lower degrees of crustal extraction (<83%) are not tolerated, as there is insufficient Rb in the nonchondritic BSE. We assume that BSE is composed of two reservoirs: DMM and CC. However, following the extraction of continental crust from BSE, the composition of the remaining mantle is not just DMM, but is a combination of DMM and subducted material. Thus, it is not surprising the model compositions of the mantle following continental crust extraction (labeled "nonchondritic BSE minus CC"; white triangles and white diamonds) are generally more enriched than estimates of DMM. The large positive Nb anomaly in the "nonchondritic BSE minus CC" reservoir might suggest a large Nb excess in the reservoir composed of subducted material. Alternatively, this Nb excess may not be present in the mantle, but instead is hosted in an additional geochemical reservoir, the core. We show a nonchondritic BSE with a Nb/U ratio of 20 to simulate Nb-loss to the core (dashed red line), and the resulting mass balance (i.e., continental crust extraction from a nonchondritic BSE) shows a smaller Nb anomaly in the "nonchondritic BSE minus CC" reservoir (black dashed lines). Estimates for DMM are shown as gray lines [*Workman and Hart*, 2005; *Salters and Stracke*, 2004; *Boyet and Carlson*, 2006]. See section 5.2 for details. Primitive mantle is from MS95.

extraction of the current volume of continental crust (Figure 6). However, our model for BSE is incompatible-element-depleted compared to the chondrite-based model for BSE. Therefore, a much larger fraction of a nonchondritic BSE must be depleted to generate continental crust. This idea is not new. In their model of a BSE that is incompatible-element-depleted relative to the chondrite-based model, *Carlson and Boyet* [2008] find that between 74% (using the *Taylor and McLennan* [1985] continental crust) and 96% (using the *Rudnick and Gao* [2003] crust) of the mantle would have to be depleted to generate the continents. Clearly, a two-layered mantle divided at 660 km, with an upper layer composed of DMM and a lower layer composed of largely primitive material [e.g., *Jacobsen and Wasserburg*, 1979], is impossible if the BSE is depleted relative to the chondrite-based model. Instead, DMM must represent most of the mantle mass [*Boyet and Carlson*, 2006; *Carlson and Boyet*, 2008].

[47] If BSE has the composition proposed in Table 3, we arrive at a similar conclusion (Figure 6). Here we estimate the mass fraction of a nonchondritic BSE that has to be depleted to generate the continents. We extract continental crustal (CC) from the nonchondritic BSE, leaving behind DMM. The mass of the mantle composed of DMM can be estimated from mass conservation [*Carlson and Boyet*, 2008]:

$$[X]_{\text{Nonchondritic BSE}}(M_{\text{CC}} + M_{\text{DMM}}) = [X]_{\text{CC}} M_{\text{CC}} + [X]_{\text{DMM}} M_{\text{DMM}} \quad (1)$$

where $[X]$ is the concentration of element X in the nonchondritic BSE, DMM, or CC, and M is the mass of the reservoir. M_{CC} is 0.555% of BSE's mass [*Galer et al.*, 1989], $[X]_{\text{CC}}$ is from *Rudnick and Gao* [2003], and $[X]_{\text{Nonchondritic BSE}}$ is from Table 3. M_{DMM} is varied until $[X]_{\text{DMM}} = 0$, which sets the minimum mass of the mantle that must be depleted to generate the continents. Rb exhibits the greatest relative difference in concentration between continental crust and DMM and plays the limiting role when determining the minimum mass of mantle that must be depleted to generate the continents. If M_{DMM} is less than 83% of the mass of the nonchondritic BSE, there is insufficient Rb to match the Rb in the continents. Therefore, at least 83% of a nonchondritic BSE must participate in continental crust extraction, and the entire mantle provides an upper limit for the mass of mantle that can be depleted to generate the continents.

[48] Using 83% of BSE as the minimum mass of DMM, equation (1) is solved to determine $[X]_{\text{DMM}}$ for a standard suite of incompatible trace elements. A spidergram for the composition of DMM after continental crust extraction from 83% of a nonchondritic BSE is shown in Figure 6 (open triangles). A spidergram for the composition of DMM after continental crust extraction from 99.455% of the mantle is also shown (Figure 6, open diamonds). These two spidergrams for DMM are generally more enriched than published estimates DMM, particularly for Nb (Figure 6). One explanation for this may be that the nonchondritic BSE is composed of three reservoirs, not two, including CC, DMM, and a reservoir composed of subducted

slab material. Therefore, after extracting continental crust [from *Rudnick and Gao*, 2003] from the nonchondritic BSE, the composition of the mantle that remains is not composed of just DMM, as is often assumed [e.g., *Carlson and Boyet*, 2008], but instead must be composed of a combination of DMM and a subducted slab component. Thus, the overall enrichment in the calculated spidergrams (Figure 6, open diamonds and triangles), in particular Nb, relative to published estimates of DMM can be attributed to the presence of a subducted component that, together with DMM, resides in the residual mantle following continental crust extraction. If so, the calculated spidergrams in Figure 6 represent a combination of DMM and subducted slab material. It is not possible to deconvolve the relative contributions of the DMM component from the subducted slab component in the calculated spidergrams in Figure 6, as the mass of subducted material in the mantle is unknown. These mass balance arguments are also considered by *Caro and Bourdon* [2010].

[49] We note that the excess Nb in the calculated spidergrams might be attributed to a subducted slab component, as subducted slabs may comprise a Nb-rich reservoir in the mantle [e.g., *McDonough*, 1991; *Rudnick et al*., 2000; *Kamber and Collerson*, 2000]. Alternatively, Nb may be concentrated in the core such that it does not contribute to BSE [*Wade and Wood*, 2001]. In this case, the Nb/U ratio of the nonchondritic BSE is lowered to a value ($\sim$20) that removes much of the excess Nb in the mantle that remains following continental crust extraction (Figure 6). Such a low BSE Nb/U ratio is lower than the value of 47–51 suggested from the OIB database in Table 2, and lower than the lowest Nb/U ratio measured (47.6) on fresh Baffin Island glasses [*Starkey et al*., 2009]. Such a low ratio is untenable if Baffin Island lavas represent melts of a nonchondritic BSE reservoir, and we consider a low Nb/U ratios of 20 for BSE to be unlikely. Balancing the Earth's Nb budget is an old and persistent problem that also afflicts the chondritic-based model for BSE of MS95, and we introduce no new explanations for this Nb problem.

[50] We note that *Huang et al*. [2013] argue that the $^{143}Nd/^{144}Nd$ isotope systematics of continental crust and DMM do not permit extraction from the nonchondritic BSE presented here (Table 1). However, we suggest that the uncertainties in their model are to too great to support their conclusions. The standard [*Jacobsen and Wasserburg*, 1980a; *Huang et al*., 2013] model that assumes continental crust derives only from the upper mantle predicts modern day $\varepsilon^{143}Nd$ values for average DMM that are about 2 to 5 ε-units lower than predicted by the nonchondritic Earth models where the DMM constitutes >70% of the mantle. However, we note that average continental crust, at the same mean age, also has an $\varepsilon^{143}Nd$ about 3 ε-units higher if generated from a nonchondritic BSE because of the higher $\varepsilon^{143}Nd$ at any given time in the nonchondritic BSE compared to the chondritic BSE undergoing continent extraction [see *Jackson and Carlson*, 2012, Figure 2]. The *Taylor and McLennan* [1985] and *Rudnick and Gao* [2003] average CC compositions differ in $\varepsilon^{143}Nd$ by 4 ε-units at the same mean age of 2 Ga. Thus, the uncertainty in average continental composition does not allow us to resolve which model, continental extraction from a chondritic BSE or a nonchondritic BSE, better approximates the evolution of the crust-mantle system.

[51] The $^{143}Nd/^{144}Nd$ evolution of DMM can also be used to constrain the evolution of the crust-mantle system. If one assumes a mean continental crust age of 2 Ga [*Huang et al*., 2013] and the crust is extracted from a mantle that starts with a chondritic Sm/Nd ratio that constitutes a volume equal to just the upper mantle, the present-day DMM will have an $\varepsilon^{143}Nd$ between +4.6 [*Taylor and McLennan*, 1985] and +7.5 [*Rudnick and Gao*, 2003]. The same approach starting from the nonchondritic BSE results in DMM $\varepsilon^{143}Nd$ near +9, assuming either the *Taylor and McLennan* [1985] average continent composition and that DMM is 74% of the mantle, or using *Rudnick and Gao* [2003] average continental crust and a DMM volume of 94% of the mantle [*Carlson and Boyet*, 2008]. Increasing the DMM volume to 90% using the *Taylor and McLennan* [1985] crustal composition decreases the predicted DMM $\varepsilon^{143}Nd$ only by half an epsilon unit. Previous estimates [e.g., *Salters and Stracke*, 2004] of the average $\varepsilon^{143}Nd$ of DMM ranged to values even higher (>+9) than those predicted by the nonchondritic BSE model. However, *Gale et al*. [2013] suggested that average DMM has an $\varepsilon^{143}Nd$ of only +8.7–8.9, a value between those predicted for DMM from a chondritic or nonchondritic starting mantle. We note that the *Gale et al*. [2013] estimate includes all MORB isotope compositions, including enriched (E) MORB, in the DMM average, which includes MORB sampling recycled continental crust (which should not be included in the average DMM composition) and MORB sampling recycled oceanic crust. Recycled oceanic crust will have enriched

(lower) $^{143}Nd/^{144}Nd$ than the average DMM peridotite and will also tend to contribute disproportionately more melt than the less-fertile DMM peridotite under the same melting conditions. Thus, including E-MORB sampling recycled oceanic crust will bias MORB averages to lower $^{143}Nd/^{144}Nd$ than the average upper mantle. For these reasons, we conclude that the average Nd-isotopic compositions of the DMM reservoir is not known precisely enough to exclude either the chondritic BSE or the nonchondritic BSE evolution models.

5.3. Consequences of a Nonchondritic BSE for Earth's Thermal History

[52] Our nonchondritic BSE model has ~30% less K, Th, and U than the chondrite-based model for BSE of MS95 and, thus, predicts a smaller contribution from radiogenic heating to Earth's thermal history. Indeed, assuming that mantle stirring by plate tectonics carries 39 TW of cooling (i.e., global cooling less cooling of the continents) through the ocean basins [*Jaupart et al*., 2007], the present day ratio of radiogenic heating to this cooling, the convective Urey number (Ur), is ~0.17, which is close to half of the preferred value of 0.33 found from a recent and exhaustive review of Earth's present-day heat budget assuming a chondritic Earth [*Jaupart et al*., 2007] (the full range is 0.21–0.49). It is well known that the relatively large convective heat flux implied by such a low Ur can be anathema to parameterized mantle thermal history models [*Korenaga*, 2008a]. For example, backward integrating classical scaling laws in which the surface heat flux carried by plate tectonics increases with internal mantle temperature will cause a "thermal catastrophe" in the form of global mantle melting within ~1–2 Gyr [*Christensen*, 1985]. Clearly, the Earth did not undergo such an event and thus our non-chondritic BSE compositional model places new demands, as well as constraints, on the mechanics and heat transfer properties of mantle convection.

[53] Thermal catastrophes are predicted where the current "mobile lid" mode of mantle convection is assumed to be a characteristic feature of the full extent of Earth history, which is almost assuredly not the case [e.g., *Grigné* et al., 2005; *Jaupart et al*., 2007; *Korenaga*, 2008a, 2008b; *Höink* et al., 2011]. Recently, *Höink et al*. [2011] find that the dynamics and heat transfer properties of plate motions depend on the average wavelength of oceanic plates relative to the mantle depth (plate aspect ratio), as well as on the mantle viscosity. Each of these factors depends strongly on the interior mantle temperature and is, thus, influenced by the magnitude of radiogenic heat production implied by our BSE model. In more detail, the motions of large plates such as the Pacific are expected to be in the "mobile lid" regime driven by conventional slab-pull physics. For small plates such as the Atlantic or for the relatively high internal mantle temperatures of the geological past, however, plate motions are predicted to be predominantly in a "sluggish lid" regime. In this case, plates are driven as a result of viscous coupling to vigorous flow within the asthenosphere driven as a result of lateral temperature variations arising because of an approximately constant surface temperature and a lithospheric thickness that increases with age. An important difference to the mobile lid heat transfer mode is that the surface heat flux increases rather than decreases as the mantle cools and becomes more viscous.

[54] At present, Earth's mantle is predominantly in a mobile lid regime, cooled mostly by the subduction and stirring of the extensive Pacific plate. A key issue for Earth's thermal history, however, is to recognize that plate motions in both regimes coexist and that the global average surface heat flux carried by mantle flow is modulated by the relative contributions of the two modes, which will evolve in response to the mantle internal temperature [*Höink et al*., 2011; *Crowley et al*., 2011]. In particular, the sluggish lid regime is favored for hotter, low viscosity mantles and plausibly governed cooling of Earth's mantle over the first billion years of Earth history. *Höink et al*. [2011] show, for example, that roughly equal contributions of cooling by mobile lid and sluggish lid modes can explain a present day mantle potential temperature in the range 1350–1400°C and $Ur = 0.33$ for a chondritic Earth.

[55] Before exploring the thermal history implications of a current $Ur = 0.17$ it is important to revisit the role of continents in the problem of mantle cooling. In typical thermal history calculations the major effect of continents is to reduce the surface heat flux carried by plate tectonics as well as the radiogenic heat production in the mantle, depending on the CC volume. *Lenardic et al*. [2011a], however, show that this approach misses the most important effect of continents, which is to insulate the mantle. Building on earlier work [*Lenardic et al*., 2005; *Jellinek and Lenardic*, 2009; *Lenardic et al*. 2011b], *Lenardic et al*. [2011a] show that continental insulation governs

the interior mantle temperature, which, in turn, determines the mantle viscosity and the rate of subduction and mantle overturning. The greater is the rate of continental radiogenic heat production, the higher will be the mantle internal temperature. Indeed, *Lenardic et al*. [2011a] show that, the most accurate way to include the ~7 TW currently carried through the continents [*Rudnick and Gao*, 2003; *Jaupart et al*., 2007] in thermal history models is to add this heat flow back into the mantle as additional heat production. Quantitatively, the effective present day Ur then increases from ~0.33 to around 0.5. Applied to our model for a nonchondritic BSE, the effective Ur increases from ~0.17 to about 0.35.

[56] To satisfy the constraints of a present day mantle potential temperature of 1350°C and an effective Ur = 0.35 with our nonchondritic BSE model, we take the initial mantle temperature to be in the range 1575–1800°C (1848–2073 K, which assumes a secular cooling rate of 50–100 K/Gyr) [*Jaupart et al*., 2007] and integrate forward in time, while varying the relative contributions of sluggish and mobile lid convective modes to the total cooling (cf. *Höink et al*., 2011; T. Höink et al., Earth's thermal evolution with multiple convection modes: A Monte-Carlo Approach, in press. *Physics of the Earth and Planetary Interiors*, 2013). To explain the present day Ur and mantle interior temperature, we require 65–80% of Earth's mantle cooling to be governed by the sluggish lid mode of convection, which is not inconsistent with expectations from modeling studies that suggest that this mode is favored over the first 1–2 Gyr of Earth history [*Korenaga*, 2008b; *Höink et al*., 2011] (Figure 7, top). In light of historical difficulties with low Ur conditions, an important inference from this thermal modeling exercise is that our nonchondritic BSE compositional model presents no dire consequences for the mantle's thermal evolution.

[57] A further remark is that our nonchondritic BSE model is inherently more demanding of thermal history models than traditional chondrite-based BSE compositions. If we perform similar calculations neglecting the insulating effects of continents, to satisfy the current mantle potential temperature and Ur = 0.17, we require >90% of Earth's cooling to be by sluggish lid convection. This picture is inconsistent with the results of modeling studies that suggest that mobile lid tectonic style is favored for plausible mantle thermal conditions over the last 1–2 Gyr [*O'Neill et al*., 2007; *Korenaga*, 2008b; *Höink et al*., 2012]. In addition, plate reconstructions and global geodynamic models suggest that mobile lid style tectonics probably governed the formation and breakup of the supercontinents Pangea, Rodinia and possibly Nuna and Kenorland over the last 1–2.5 Gyr [*Li and Zhong*, 2009].

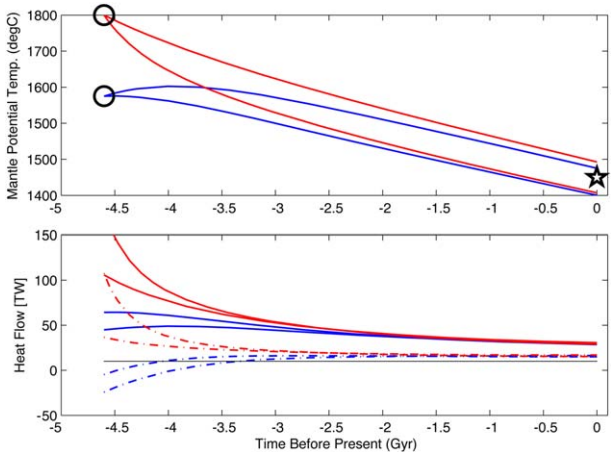

Figure 7. (top) Thermal evolution of the nonchondritic BSE (from Table 3) from initial temperatures (large circles) assuming either a secular cooling rate of 50 K/Gyr (blue curves) or 100 K/Gyr (red curves) [e.g., *Jaupart et al*., 2007] and an effective Ur = 0.35 that incorporates the insulating effects of continents. The heat flow carried out of the mantle by plate tectonics is a strong function of plate size (wavelength), which is expected to decline back through geological time with increasing mantle interior temperature [*Höink et al*., 2011]. The surface heat flow at any time can, thus, be decomposed into time-varying contributions from large plates such as the Pacific in the "mobile lid" regime and small plates such as the Atlantic in the "sluggish lid regime." To satisfy a present day mantle potential temperature of 1350°C (star) our BSE requires that the sluggish lid mode carry 65% (lower solid red and blue lines) to 80% (upper solid red and blue lines) of the total mantle. (bottom) Time series showing the evolution of surface convective heat flow (solid lines) and the core heat flow (dash-dot lines) for the high (red curves) and low (blue curves) initial mantle temperatures. The solid black line indicates the critical core-mantle boundary heat flow required for a thermally driven dynamo to operate. As with the thermal histories (top), the envelopes defined by the upper and lower curves of the same color and line type indicate the upper and lower bounds on the contribution of the sluggish lid mode of mantle convection to total mantle cooling. See section 5.3 of the text for discussion.

[58] A final issue to consider briefly is the extent to which the evolution in mantle convective heat flow we require to satisfy the current effective Ur and mantle interior temperature is consistent with a predominantly thermally driven dynamo over the 1–2 billion years of Earth's evolution [*Labrosse et al*., 2001] (Figure 7, bottom). Taking 10

TW to be a reasonable critical core-mantle boundary heat flux for dynamo action [e.g., *Buffett*, 2002; *Christensen and Aubert*, 2006], for the very high initial mantle temperature of 1800°C, a dynamo is possible over the full extent of our thermal history calculations. However, for the more reasonable initial temperature of 1575°C, dynamo action is not possible until 3.9–3.5 Gyr and, moreover, the mantle may heat the core over the first ~500 myr of Earth evolution. Although our model is crude, the delayed onset of dynamo action required by our nonchondritic BSE is consistent with the 3.4–3.45 Gyr dynamo age inferred from single crystal paleointensity measurements [*Tarduno et al*., 2010] as well as from the delivery of terrestrial nitrogen to lunar far side soils [*Ozima et al*., 2005].

6. Conclusions

[59] We draw the following conclusions from this study:

(1) The lithophile element composition of a nonchondritic BSE is assumed to have a present-day make-up similar to the high $^{3}He/^{4}He$ mantle. The nonchondritic BSE has Sm/Nd ~6% higher than chondritic and a present-day $^{143}Nd/^{144}Nd$ of 0.5130; it is consistent with the $^{142}Nd/^{144}Nd$ difference between Earth and the O-chondrite reservoir, and is an alternative composition to the traditional chondritic-based BSE.

(2) We present major and trace element concentrations for the high $^{3}He/^{4}He$ mantle, which represents the composition of the nonchondritic BSE. The concentrations of highly incompatible elements (Rb, Ba, Th, U, K, etc) are ~30% lower than a chondrite-based BSE. There are several implications for an incompatible element depleted BSE composition:
   A. Continental crust must be extracted from >83% of the BSE. If <83% of a nonchondritic BSE is depleted, there is insufficient Rb to generate the continents.
   B. Our nonchondritic BSE has a lower K concentration that permits a lower ^{40}Ar budget in the solid Earth and atmosphere. The ^{40}Ar in the atmosphere, continental crust and DMM may be sufficient to balance the Ar budget for our proposed low-K BSE, thus obviating the need for a "missing" ^{40}Ar reservoir and providing a solution to the missing Ar paradox.
   C. Melt models of the nonchondritic BSE, which is here thought to be represented by the lithophile element composition of the high $^{3}He/^{4}He$ mantle, generate trace element patterns similar to the highest $^{3}He/^{4}He$ basalt globally.

(3) From our thermal history models, our new BSE has three key implications. First, Earth's thermal history can be readily characterized with our nonchondritic model without requiring a thermal catastrophe in the recent past. Second, for realistic initial mantle temperatures the lower rate of heat production requires that mantle convection cool the Earth in predominantly a small plate/sluggish lid mode over more than half of Earth's early evolution. That is, the classical Pacific plate-style of plate tectonics driven by slab-pull physics was not the dominant mode of mantle stirring over the first 1–2 Gyr of Earth evolution. Finally, for plausible initial mantle temperatures we expect heat transfer into the core and a delay of core convection and dynamo action until as recently as 3.5 Gyr. In summary, the lower U, Th and K concentrations calculated for a nonchondritic BSE present no dire consequences for the thermal evolution of the Earth and may provide a restrictive constraint on the age of Earth's magnetic field.

Acknowledgments

[62] This paper is dedicated to Karl Turekian, who introduced Jackson to the "missing" Ar problem in his first geochemistry course as an undergraduate. The course (and Karl) was inspirational, and the rest was history! We thank Rick Carlson for invaluable advice on continental crust extraction models. We also thank Stan Hart, Nobu Shimizu and Steve Shirey for discussion. Dave Graham and Bernard Bourdon provided insightful and helpful comments. We thank the "Bills" (McDonough and White) and an anonymous reviewer for comments on an earlier version of the manuscript. MGJ was supported by NSF grants OCE-1061134 and EAR-1145202. AMJ was supported by NSERC and the Canadian Institute for Advanced Research.

References

Albarède, F. (1998), Time-dependent models of U–Th–He and K–Ar evolution and the layering of mantle convection, *Chem. Geol.*, *145*, 413–429.

Allègre, C. J., D. B. Othman, M. Polve, and D. Richard (1979), Nd–Sr isotopic correlation in mantle materials and geodynamic consequences, *Phys. Earth Planet. Inter.*, *19*, 293–306.

Allègre, C. J., A. Hofmann, and K. O'Nions (1996), The argon constraints on mantle structure, *Geophys. Res. Lett.*, *23*, 3555–3557.

Andreasen, R., and M. Sharma (2006), Solar nebula heterogeneity in p-process samarium and neodymium isotopes, *Science*, *314*, 806–809.

Andreasen, R., and M. Sharma (2007), Mixing and homogenization in the early solar system: Clues from Sr, Ba, Nd and Sm isotopes in meteorites, *Astrophys. J.*, *665*, 874–883.

Andreasen, R., M. Sharma, K. V. Subbarao, and S. G. Viladkar (2008), Where on Earth is the enriched Hadean reservoir?, *Earth Planet. Sci. Lett.*, *266*, 14–28.

Arevalo, R., W. F. McDonough, and M. Luong (2009), The K/U ratio of the silicate Earth: Insights into mantle composition, structure and thermal evolution, *Earth Planet. Sci. Lett.*, *278*, 361–369.

Bouvier, A., J. D. Vervoort, and P. J. Patchett (2008), The Lu–Hf and Sm–Nd isotopic composition of CHUR: Constraints from unequilibrated chondrites and implications for the bulk composition of terrestrial planets, *Earth Planet. Sci. Lett.*,*273*, 48–57.

Boyet, M., and R. W. Carlson (2005), ^{142}Nd evidence for early (>4.53 Ga) global differentiation of the silicate Earth, *Science*, *309*, 576–581.

Boyet, M., and R.W. Carlson (2006), A new geochemical model for the Earth's mantle inferred from ^{146}Sm–^{142}Nd systematics, *Earth Planet. Sci. Lett.*, *250*, 254–268.

Brandenburg, J. P., E. K. Hauri, P. E. van Keken, and C. J. Ballentine (2008), A multiplesystem study of the geochemical evolution of the mantle with force-balanced plates and thermochemical effects, *Earth Planet. Sci. Lett.*, *276*, 1–13.

Buffett, B. A. (2002), Estimates of heat flow in the deep mantle based on the power requirements for the geodynamo, *Geophys. Res. Lett.*, *29*(12), 1566, doi:10.1029/2001GL014649.

Carlson, R. W., and M. Boyet (2008), Composition of the Earth's interior: The importance of early events, *Philos. Trans. R. Soc. A*, *366*, 4077–4103.

Carlson, R. W., M. Boyet, and M. Horan (2007), Chondrite barium, neodymium, and samarium isotopic heterogeneity and early earth differentiation, *Science*, *316*, 1175–1178.

Caro, G., and B. Bourdon (2010), Non-chondritic Sm/Nd ratio in the terrestrial planets: Consequences for the geochemical evolution of the mantle–crust system, *Geochim. Cosmochim. Acta*, *74*, 3333–3349.

Caro, G., B. Bourdon, J. L. Birck, and S. Moorbath (2006), High precision ^{142}Nd/^{144}Nd measurements in terrestrial rocks: Constraints on the early differentiation of the Earth's mantle, *Geochim. Cosmochim. Acta*, *70*, 164–191.

Caro, G., B. Bourdon, A. N. Halliday, and G. Quitte (2008), Super-chondritic Sm/Nd ratios in Mars, the Earth and the Moon, *Nature*, *452*, 336–339.

Chabot, N. L., and M. J. Drake (1999), Potassium solubility in metal: The effects of composition at 15 kbar 1900°C on partitioning between iron alloys and silicate melts, *Earth Planet. Sci. Lett.*, *172*, 323–335.

Chauvel, C., and J. Blichert-Toft (2001), A hafnium isotope and trace element perspective on melting, of the depleted mantle, *Earth Planet. Sci. Lett.*, *190*, 137–151.

Chauvel, C., E. Lewin, M. Carpentier, N. T. Arndt, and J. C. Marini (2008), Role of recycled oceanic basalts and sediments in generating the Hf–Nd mantle array, *Nat. Geosci.*, *1*, 64–67.

Christensen, U. R. (1985), Thermal evolution models for the Earth, *J. Geophys. Res.*, *90*, 2995–3007.

Christensen, U. R., and J. Aubert (2006), Scaling properties of convection-driven dynamos in rotating spherical shells and application to planetary magnetic fields, *Geophys. J. Int.*, *166*, 97–114.

Class, C., and S. L. Goldstein (2005), Evolution of helium isotopes in the Earth's mantle, *Nature*, *436*, 1107–1112.

Craig, H., W. Clarke, and M. Begg (1975), Excess ^{3}He in deep water on the East Pacific Rise, *Earth Planet. Sci. Lett.*, *26*, 125–134.

Crowley, J. W., M. Gérault, and R. J. O'Connell (2011), On the relative influence of heat and water transport on planetary dynamics, *Earth Planet. Sci. Lett.*, *310*, 380–388.

Davies, G. F. (1999), Geophysically constrained mantle mass flows and the ^{40}Ar budget: A degassed lower mantle?, *Earth Planet. Sci. Lett.*, *166*, 149–162.

DePaolo, D. J. (1980), Crustal growth and mantle evolution: Inferences from models of element transport and Sr and Nd isotopes, *Geochim. Cosmochim. Acta*, *44*, 1185–1196.

DePaolo, D. J., and G. J. Wasserburg (1979), Petrogenetic mixing models and Nd–Sr isotopic patterns, *Geochim. Cosmochim. Acta*, *43*, 615–627.

Farley, K., E. Maier-Reimer, P. Schlosser, and W. Broecker (1995), Constraints on mantle ^{3}He fluxes and deep-sea circulation from an oceanic general circulation model, *J. Geophys. Res.*, *100*, 3829–3839.

Farley, K. A., J. H. Natland, and H. Craig (1992), Binary mixing of enriched and undegassed (primitive?) mantle components (He, Sr, Nd, Pb) in Samoan lavas, Earth Planet. *Sci. Lett.*, *111*, 183–199.

Gale, A., C. A. Dalton, C. H. Langmuir, Y. Su, and J.-G. Schilling (2013), The mean composition of ocean ridge basalts, *Geochem. Geophys. Geosyst.*, *14*, 489–518, doi:10.1029/2012GC004334.

Galer, S. J. G., S. L. Goldstein, and R. K. O'Nions (1989), Limits on chemical and convective isolation in the Earth's interior, *Chem. Geol.*, *75*, 257–290.

Gannoun, A., M. Boyet, H. Rizo, and A. El Goresy (2011), ^{146}Sm–^{142}Nd systematics measured in enstatite chondrites reveals a heterogeneous distribution of ^{142}Nd in the solar nebula, *Proc. Natl. Acad. Sci. U. S. A.*, *108*, 7693–7697, doi:10.1073/pnas.1017332108.

Gast, P. W. (1968), Trace element fractionation and the origin of tholeiitic and alkaline magma types, *Geochim. Cosmochim. Acta*, *32*, 1057–1086.

Gessmann, C. K., and B. J. Wood (2002), Potassium in the Earth's core?, *Earth Planet. Sci. Lett.*, *200*, 63–78.

Gonnermann, H. M., and S. Mukhopadhyay (2007), Non-equilibrium degassing and a primordial source for helium in ocean-island volcanism, *Nature*, *449*, 1037–1040.

Gonnermann, H. M., and S. Mukhopadhyay (2009), Preserving noble gases in a convecting mantle, *Nature*, *459*, 560–563.

Graham, D. W. (2002), Noble gas isotope geochemistry of mid-ocean ridge and ocean island basalts; characterization of mantle source reservoirs, in *Noble Gases in Geochemistry and Cosmochemistry, Rev. in Mineral. and Geochem.*, vol. 47, edited by D. Porcelli, C. J. Ballentine, and R. Wieler, pp. 247–318, Mineral. Soc. of Am., Washington, D. C.

Graham, D. W., L. M. Larsen, B. B. Hanan, M. Storey, A. K. Pedersen, and J. E. Lupton (1998), Helium isotope composition of the early Iceland mantle plume inferred from the Tertiary picrites of West Greenland, *Earth Planet. Sci. Lett.*, *160*, 241–255.

Grigné, C., S. Labrosse, and P. J. Tackley (2005), Convective heat transfer as a function of wavelength: Implications for the cooling of the Earth, *J. Geophys. Res.*, *110*, B03409, doi:10.1029/2004JB003376.

Hanan, B. B., and D. W. Graham (1996), Lead and helium isotope evidence from oceanic basalts for a common deep

source of mantle plumes, *Science*, *272*, 991–995, doi:10.1126/science.272.5264.991.

Hart, S. R., and A. Zindler (1986), In search of a bulk-Earth composition, *Chem. Geol.*, *57*, 247–267.

Hart, S. R., and G. A. Gaetani (2006), Mantle Pb paradoxes: The sulfide solution, *Contrib. Mineral. Petrol.*, *152*, 295–308.

Hart, S. R., E. H. Hauri, L. A. Oschmann, and J. A. Whitehead (1992), Mantle plumes and entrainment: Isotopic evidence, *Science*, *256*, 517–520, doi:10.1126/science.256.5056.517.

Herzberg, C., and E. Gazel (2009), Petrological evidence for secular cooling in mantle plumes, *Nature*, *458*, 619–622.

Hofmann, A. W. (1988), Chemical differentiation of the Earth: The relationship between mantle, continental crust, and oceanic crust, *Earth Planet. Sci. Lett.*, *90*, 297–314.

Hofmann, A.W. (1997), Mantle geochemistry: The message from oceanic volcanism, *Nature*, *365*, 219–229.

Hofmann, A. W. (2003) Sampling mantle heterogeneity through oceanic basalts: Isotopes and trace elements, in *Treatise on Geochemistry*, vol. *2*, The Mantle and Core, edited by H. D. Holland and K. K. Turekian, pp. 61–101, Elsevier, Oxford, U. K.

Hofmann, A. W., and W. M. White (1983), Ba, Rb and Cs in the Earth's Mantle, *Z. Naturforsch*, *38*(a), 256–266.

Hofmann, A. W., K. P. Jochum, M. Seufert, and W. M. White (1986), Nb and Pb in oceanic basalts: New constraints on mantle evolution, *Earth Planet. Sci. Lett.*, *79*, 33–45.

Höink, T., A. M. Jellinek, and A. Lenardic (2011), Viscous coupling at the lithosphere-asthenosphere boundary, *Geochem. Geophys. Geosyst. 12*, Q0AK02. doi:10.1029/2011GC003698.

Höink, T., A. Lenardic, and M. Richards (2012), Depth-dependent viscosity and mantle stress amplification: Implications for the role of the asthenosphere in maintaining plate tectonics, *Geophys. J. Int.*, *191*, 30–41.

Honda, M., and D. B. Patterson (1999), Systematic elemental fractionation of mantle-derived helium, neon, and argon in mid-oceanic ridge glasses, *Geochim. Cosmochim. Acta*, *63*, 2863–2874.

Huang, S., S. B. Jacobsen, and S. Mukhopadhyay (2013), ^{147}Sm-^{143}Nd systematics of Earth are inconsistent with a superchondritic Sm/Nd ratio, *Proc Natl. Acad. Sci.*, *110*, doi:10.1073/pnas.1222252110.

Jackson, M. G., and R. W. Carlson (2011), An ancient recipe for flood-basalt genesis, *Nature*, *476*, 316–319.

Jackson, M. G., and R. W. Carlson (2012), Homogeneous superchondritic ^{142}Nd/^{144}Nd in the mid-ocean ridge basalt and ocean island basalt mantle, *Geochem. Geophys. Geosyst.*, *13*, Q06011, doi:10.1029/2012GC004114.

Jackson, M. G., M. D. Kurz, S. R. Hart, and R. K. Workman (2007), New Samoan lavas from Ofu Island reveal a hemispherically heterogeneous high ^{3}He/^{4}He mantle, *Earth Planet. Sci. Lett.*, *264*, 360–374.

Jackson, M. G., S. R. Hart, A. E. Saal, N. Shimizu, M. D. Kurz, J. S. Blusztajn, and A. S. Skovgaard (2008), Globally elevated titanium, tantalum, and niobium (TITAN) in ocean island basalts with high ^{3}He/^{4}He, *Geochem. Geophys. Geosyst*, *9*, Q04027, doi:10.1029/2007GC001876.

Jackson, M. G., R. W. Carlson, M. D. Kurz, P. D. Kempton, P. D. Francis, and J. Blusztajn (2010), Evidence for the survival of the oldest terrestrial mantle reservoir, *Nature*, *466*, 853–856.

Jacobsen, S. B., and G. J. Wasserburg (1979), The mean age of mantle and crustal reservoirs, *J. Geophys. Res.*, *84*, 7411–7427.

Jacobsen, S. B. and G. J. Wasserburg (1980a), A two-reservoir recycling model for mantle-crust evolution, *Proc. Natl. Acad. Sci. U. S. A.*, *77*, 6298–6302.

Jacobsen, S. B., and G. J. Wasserburg (1980b), Sm–Nd isotopic evolution of chondrites, *Earth Planet. Sci. Lett.*, *50*, 139–155.

Jaupart, C., S. Labrosse, and J.-C. Mareschal (2007), Temperatures, heat and energy in the mantle of the Earth, in *Treatise on Geophysics*, vol. *7*, edited by G. Schubert, pp. 253–304, Elsevier, Oxford.

Javoy, M., et al. (2010), The chemical composition of the Earth: Enstatite chondrite models, *Earth Planet. Sci. Lett.*, *293*, 259–268.

Jellinek, A. M., and A. Lenardic (2009), Effects of spatially-varying roof cooling on Benard convection in a fluid with a temperature-dependent viscosity, *J. Fluid Mech.*, *629*, 109–137.

Jochum, K. P., A. W. Hofmann, E. Ito, H. M. Seufert, and W. M. White (1983), K, U and Th in mid-ocean ridge basalt glasses and heat-production, K/U and K/Rb in the mantle, *Nature*, *306*, 431–436.

Kamber, B. S., and K. D. Collerson (2000), Role of ''hidden'' deeply subducted slabs in mantle depletion, *Chem. Geol.*, *166*, 241–254.

Kinoshita, N., et al. (2012), A shorter ^{146}Sm half-life measured and implications for ^{146}Sm-^{142}Nd chronology of the solar system, *Science*, *335*, 1614–1617, doi:10.1126/science.1215510.

Kleine, T., C. Burkhardt, and P. Sprung (2013), Chondritic Sm/Nd in terrestrial planets and the origin of nucleosynthetic 142Nd variations, in Proceedings of 44th Lunar and Planetary Science Conference, pp. 3020–3021, Lunar and Planet. Inst., Houston, Tex.

Korenaga, J. (2008a), Urey ratio and the structure and evolution of Earth's mantle, *Rev. Geophys.*, *46*, RG2007, doi:10.1029/2007RG000241.

Korenaga, J. (2008b), Plate tectonics, flood basalts and the evolution of Earth's oceans, *Terra Nova*, *20*, 419–439.

Kurz, M. D., W. J. Jenkins, and S. R. Hart (1982), Helium isotopic systematics of oceanic islands and mantle heterogeneity, *Nature*, *297*, 43–47.

Kurz, M. D., W. J. Jenkins, S. R. Hart, and D. Clague (1983), Helium isotopic variations in volcanic rocks from Loihi Seamount and the Island of Hawaii, *Earth Planet. Sci. Lett.*, *66*, 388–406.

Labrosse, S., J. P. Poirier, and J. L. Le Mouël (2001), The age of the inner core, *Earth Planet. Sci. Lett.*, *190*, 111–123.

Labrosse, J. W., J. Hernlund, and N. Coltice (2007), A crystallizing dense magma ocean at the base of Earth's mantle, *Nature*, *450*, 866–869.

Lassiter, J. C. (2004), Role of recycled oceanic crust in the potassium and argon budget of the Earth: Toward a resolution of the ''missing argon'' problem, *Geochem. Geophys. Geosyst.*, *5*, Q11012, doi:10.1029/2004GC000711.

Lenardic, A., L. N. Moresi, A. M. Jellinek, and M. Manga (2005), Continental insulation, mantle cooling, and the surface area of oceans and continents, *Earth Planet. Sci. Lett.*, *234*, 317–333.

Lenardic, A., C. M. Cooper, and L. Moresi (2011a), A note on continents and the Earth's Urey ratio, *Phys. Earth Planet. Inter.*, *188*, 127–130.

Lenardic, A., L. Moresi, A. M. Jellinek, C. J. O'Neill, C. M. Cooper, and C. T. Lee (2011b), Continents, supercontinents, mantle thermal mixing, and mantle thermal isolation: Theory, numerical simulations, and laboratory experiments, *Geochem. Geophys. Geosyst.*, *12*, Q10016, doi:10.1029/2011GC003663.

Li, Z. X., and S. Zhong (2009), Supercontinent–superplume coupling, true polar wander and plume mobility: Plate

dominance in whole-mantle tectonics, *Phys. Earth Planet. Inter.*, *176*, 143–156.
Lodders, K. (1995), Alkali elements in the Earth's core—Evidence from enstatite meteorites, *Meteoritics*, *30*, 93–101.
Lyubetskaya, T., and J. Korenaga (2007), Chemical composition of Earth's primitive mantle and its variance: 2. Implications for global geodynamics, *J. Geophys. Res.*, *112*, B03212, doi:10.1029/2005JB004224.
McDonough, W. F. (1991), Partial melting of subducted oceanic crust and isolation of its residual eclogitic lithology, *Philos. Trans. R. Soc. A*, *335*, 407–418, doi:10.1098/rsta.1991.0055.
McDonough, W. F., and S. S. Sun (1995), The composition of the Earth, *Chem. Geol.*, *120*, 223–253, doi:10.1016/0009–2541(94)00140-4.
Moreira, M., J. Kunz, and C. Allègre (1998), Rare gas systematic in Popping Rock: Isotopic and elemental compositions in the upper mantle, *Science*, *279*, 1178–1181.
Mukhopadhyay, S. (2012), Early differentiation and volatile accretion recorded in deep-mantle neon and xenon, *Nature*, 486, 101–104, doi:10.1038/nature11141.
Murphy, D. T., A. D. Brandon, V. Debaille, R. Burgess, and C. Ballentine (2010), $^{142}Nd/^{144}Nd$ reservoir in the deep mantle: Implications for the Nd isotope systematics of the Earth, *Geochim. Cosmochim. Acta*, *74*, 738–750.
O'Neill, H. S. C., and H. Palme (1998), Composition of the silicate Earth: Implications for accretion and core formation, in *The Earth's Mantle: Structure, Composition, and Evolution, The Ringwood Volume*, edited by I. Jackson, pp. 3–126, Cambridge Univ. Press, New York.
O'Neill, H. S. C., and H. Palme (2008), Collisional erosion and the non-chondritic composition of the terrestrial planets, *Philos. Trans. R. Soc. A*, *366*, 4205–4238, doi:10.1098/rsta.2008.0111.
O'Neill, C., A. Lenardic, L. Moresi, T. H. Torsvik, and C. T. Lee (2007), Episodic precambrian subduction, *Earth Planet. Sci. Lett.*, *262*, 552–562.
Ozima, M., K. Seki, N. Terada, Y. N. Miura, F. A. Podosek, and H. Shinagawa (2005), Terrestrial nitrogen and noble gases in lunar soils, *Nature*, *436*(7051), 655–659.
Palme, H., and H. S. C. O'Neil (2003), Cosmochemical estimates of mantle composition, in *Treatise on Geochemistry*, vol. 2, The Mantle and Core, edited by H. D. Holland and K. K. Turekian, pp. 1–38, Elsevier, Oxford, U. K.
Parman, S. W., M. D. Kurz, S. R. Hart, and T. L. Grove (2005), Helium solubility in olivine and implications for high $^{3}He/^{4}He$ in ocean island basalts, *Nature*, *437*, 1140–1143.
Patchett, P. J., O. Kouvo, C. E. Hedge, and M. Tatsumoto (1981), Evolution of continental crust and mantle heterogeneity: Evidence from Hf isotopes, *Contrib. Mineral. Petrol.*, *78*, 279–297.
Qin, L., R. W. Carlson, and C. M. O. Alexander (2011), Correlated nucleosynthetic isotopic variability in Cr, Sr, Ba, Sm, Nd and Hf in Murchison and QUE 97008, *Geochim. Cosmochim. Acta*, *75*, 7806–7828.
Ranen, M. C., and S. B. Jacobsen (2006), Barium isotopes in chondritic meteorites: Implications for planetary reservoir models, *Science*, *314*, 809–812, doi:10.1126/science.1132595.
Rudnick, R. L., and S. Gao (2003), Composition of the continental crust, in *Treatise on Geochemistry, The Crust*, vol. *3*, edited by R. L. Rudnick, pp. 1–64, Permagon, New York.
Rudnick, R. L., M. Barth, I. Horn, and W. F. McDonough (2000), Rutile-bearing refractory eclogites: The missing link between continents and depleted mantle, *Science*, *287*, 278–281, doi:10.1126/science.287.5451.278.
Sarda, P., and M. Moreira (2001), Vesiculation and vesicle loss in mid-ocean ridge basalt glasses: He, Ne, Ar elemental fractionation and pressure influence, *Geochim. Cosmochim. Acta*, *66*, 1449–1458.
Salters, V. J. M., and S. R. Hart (1991), The mantle sources of ocean ridges, islands and arcs: The Hf-isotope connection, *Earth Planet. Sci. Lett.*, *104*, 364–380.
Salters, V. J. M., and A. Stracke (2004), Composition of the depleted mantle, *Geochem. Geophys. Geosyst.*, *5*, Q05004, doi:10.1029/2003GC000597.
Starkey, N. A., F. M. Stuart, R. M. Ellam, J. G. Fitton, S. Basu, and L. M. Larsen (2009), Helium isotopes in early Iceland plume picrites: Constraints on the composition of high $^{3}He/^{4}He$ mantle, *Earth Planet. Sci. Lett.*, *277*, 91–100.
Storey, M., R. A. Duncan, A. K. Pedersen, L. M. Larsen, and H. C. Larsen (1998), $^{40}Ar/^{39}Ar$ geochronology of the West Greenland Tertiary volcanic province, *Earth Planet. Sci. Lett.*, 160, 569–586.
Stuart, F. M., S. Lass-Evans, J. G. Fitton, and R. M. Ellam (2003), High $^{3}He/^{4}He$ ratios in picritic basalts from Baffin Island and the role of a mixed reservoir in mantle plumes, *Nature*, *424*, 57–59.
Su, Y. (2003), Global MORB chemistry compilation at the segment scale, PhD thesis, Dept. of Earth and Environ. Sci., Columbia Univ, New York.
Sun, S., and W. F. McDonough (1989), Chemical and isotopic systematics of oceanic basalts: Implications for mantle composition and processes, in *Magmatism in the Ocean Basins*, edited by A. D. Saunders and M. J. Norry, Geol. Soc. London Spec. Publ., *42*, 313–345.
Tarduno, J. A., R. D. Cottrell, M. K. Watkeys, A. Hofmann, P. V. Doubrovine, E. E. Mamajek, and Y. Usui (2010), Geodynamo, solar wind, and magnetopause 3.4 to 3.45 billion years ago, *Science*, *327*, 1238–1240.
Taylor, S. R. and S. M. McLennan (1985), *The Continental Crust: Its Composition and Evolution*, Blackwell Sci., Oxford, U. K.
Turekian, K. K. (1959), The terrestrial economy of helium and argon, *Geochim. Cosmochim. Acta*, *17*, 37–43.
van Keken, P., C. Ballentine, and E. Hauri (2004), Convective mixing in the Earth's mantle, in *Treatise on Geochemistry*, vol. 2, The Mantle and Core, edited by H. D. Turekian and K. K. Holland, Elsevier, pp. 471–491.
Vervoort, J. D., P. J. Patchett, J. Blichert-Toft, and F. Albarède (1999), Relationships between Lu–Hf and Sm–Nd isotopic systems in the global sedimentary system, *Earth Planet. Sci. Lett.*, *168*, 79–99.
Wade, J., and B. J. Wood (2001), The Earth's 'missing' Nb may be in the core?, *Nature*, *409*, 75–78. doi:10.1038/35051064.
Wasserburg, G. J., W. A. Fowler, G. J. F. Macdonald, and F. Hoyle (1964), Relative contributions of uranium thorium+potassium to heat production in Earth, *Science*, *143*, 465–467.
White, W. M. (2010), Oceanic island basalts and mantle plumes: The geochemical perspective, *Annu. Rev. Earth Planet. Sci.*, *38*, 133–160, doi:10.1146/annurev-earth-040809–152450.
Willbold, M., and A. Stracke (2006), Trace element composition of mantle end-members: Implications for recycling of oceanic and upper and lower continental crust, *Geochem. Geophys. Geosyst*, *7*, Q04004, doi:10.1029/2005GC001005.
Workman, R. K., and S. R. Hart (2005), Major and trace element composition of the depleted MORB mantle (DMM), *Earth Planet. Sci. Lett.*, *231*, 53–72.
Zindler, A., and S. R. Hart (1986), Chemical geodynamics, *Annu. Rev. Earth Planet. Sci.*, *14*, 493–571, doi:10.1146/annurev.ea.14.050186.002425.